Radiology

Special Review

Thomas G. Flohr, PhD
Stefan Schaller, PhD
Karl Stierstorfer, PhD
Herbert Bruder, PhD
Bernd M. Ohnesorge, PhD
U. Joseph Schoepf, MD

Published online before print
10.1148/radiol.2353040037
Radiology 2005; 235:756–773

Abbreviations:
AMPR = adaptive MPR
ECG = electrocardiography
FWHM = full width at half maximum
MPR = multiplanar reformation
SSP = section-sensitivity profile
3D = three-dimensional

[1] From Siemens Medical Solutions, CT Division, Forchheim, Germany (T.G.F., S.S., K.S., H.B., B.M.O.); Department of Diagnostic Radiology, Tübingen University, Germany (T.G.F.); and Department of Radiology, Medical University of South Carolina, 169 Ashley Ave, Charleston, SC 29425 (U.J.S.). Received January 7, 2004; revision requested March 9; revision received April 26; accepted May 24. **Address correspondence to** U.J.S. (e-mail: *schoepf@musc.edu*).

U.J.S. is a medical consultant to Siemens Medical Solutions, CT Division, Forchheim, Germany.

Multi–Detector Row CT Systems and Image-Reconstruction Techniques[1]

The introduction in 1998 of multi–detector row computed tomography (CT) by the major CT vendors was a milestone with regard to increased scan speed, improved z-axis spatial resolution, and better utilization of the available x-ray power. In this review, the general technical principles of multi–detector row CT are reviewed as they apply to the established four- and eight-section systems, the most recent 16-section scanners, and future generations of multi–detector row CT systems. Clinical examples are used to demonstrate both the potential and the limitations of the different scanner types. When necessary, standard single-section CT is referred to as a common basis and starting point for further developments. Another focus is the increasingly important topic of patient radiation exposure, successful dose management, and strategies for dose reduction. Finally, the evolutionary steps from traditional single-section spiral image-reconstruction algorithms to the most recent approaches toward multisection spiral reconstruction are traced.

Supplemental material: *radiology.rsnajnls.org/cgi/content/full/2353040037/DC1*

Computed tomography (CT) was introduced in the early 1970s and has revolutionized the practice not only of diagnostic radiology but also of the whole field of medicine. CT was the first technology to marry a computer to a medical imaging machine, the first to display x-ray images as cross sections, and the first modality to herald a new era of digital imaging.

A glossary of terms used in this review is available online in Appendix E1 (*radiology.rsnajnls.org/cgi/content/full/2353040037/DC1*).

EVOLUTION OF SPIRAL CT: FROM ONE SECTION TO 16

The introduction of spiral CT in the early 1990s constituted a fundamental evolutionary step in the development and ongoing refinement of CT imaging techniques (1,2). For the first time, volume data could be acquired without misregistration of anatomic detail. Volume data became the basis for applications such as CT angiography (3), which has revolutionized the noninvasive assessment of vascular disease. The ability to acquire volume data also paved the way for the development of three-dimensional (3D) image-processing techniques such as multiplanar reformation (MPR), maximum intensity projection, surface-shaded display, and volume-rendering techniques (4), which have become a vital component of medical imaging today.

Ideally, volume data are of high spatial resolution and are isotropic in nature: Each image data element (voxel) is of equal dimensions in all three spatial axes, and this forms the basis for image display in arbitrarily oriented imaging planes. For most clinical scenarios, however, single-section spiral CT with a 1-second gantry rotation is unable to fulfill these requirements. To prevent motion artifacts and optimally utilize the contrast agent bolus, body spiral CT examinations need to be completed within a certain time frame of, ordinarily, one breath hold (25–30 seconds). If a large scan range such as the entire thorax or abdomen (30 cm) has to be covered within a single breath hold, a thick collimation of 5–8 mm must be used. While the in-plane resolution of a CT image depends on the system geometry and on the reconstruction kernel selected by the user, the

ESSENTIALS

- *Multi–detector row CT allows substantial reduction in examination time for standard protocols, coverage of extended anatomic volumes, and, most important, substantially increased longitudinal resolution by means of reduced section width.*
- *Near-isotropic spatial resolution in routine examinations, which has been achieved with 16-section CT systems, enables 3D renderings of diagnostic quality and oblique MPRs and maximum intensity projections with resolution similar to that of the transverse images.*
- *Scanning at narrow collimation does not markedly increase the radiation dose to the patient, as long as the effective milliampere-seconds level is kept constant.*
- *A key challenge for image reconstruction with multi–detector row CT is the cone angle of the measurement rays; this requires novel reconstruction techniques such as 3D back projection, AMPR, or weighted hyperplane reconstruction.*
- *Z filtering makes it possible to reconstruct images retrospectively with different section widths from the same raw CT data set, trading off, in this way, z-axis resolution and image noise.*

longitudinal (z-axis) resolution along the patient axis is determined by the collimated section width and the spiral interpolation algorithm. Use of a thick collimation of 5–8 mm results in a considerable mismatch between the longitudinal resolution and the in-plane resolution, which is 0.5–0.7 mm, depending on the reconstruction kernel. Thus, with single-section spiral CT, the ideal of isotropic resolution can only be achieved for very limited scan ranges (5).

Strategies to achieve more substantial volume coverage with improved longitudinal resolution include the simultaneous acquisition of more than one section at a time and a reduction in the gantry rotation time. Interestingly, the first medical CT scanners were two-section systems, such as the EMI (England) head scanner, introduced in 1972, and the Siemens Siretom (Erlangen, Germany), introduced in 1974. With the advent of whole-body fan-beam CT systems for general radiology, two-section acquisition was no longer used. Apart from a dedicated two-section system for cardiac applications, the Imatron C-100 (Imatron, San Francisco, Calif), which was introduced in 1984, the first step toward multisection acquisition in general radiology was a two-section CT scanner introduced in 1993 (Elscint TWIN; Elscint, Haifa, Israel) (6). In 1998, several CT manufacturers introduced multi–detector row CT systems, which provided considerable improvement in scanning speed and longitudinal resolution and better utilization of the available x-ray power (7–10). These systems typically offered simultaneous acquisition of four sections at a gantry rotation time of 0.5 second.

Simultaneous acquisition of *m* sections results in an *m*-fold increase in speed if all other parameters (eg, section thickness) are unchanged. This increased performance of multi–detector row CT relative to single-section CT allowed the optimization of a variety of clinical protocols. The examination time for standard protocols could be substantially reduced, which proved to be of immediate clinical benefit for the quick and comprehensive assessment of trauma patients and uncooperative patients (11). Alternatively, the scan range that could be covered within a certain time was extended by a factor of *m,* which is relevant for oncologic staging or for CT angiography with extended coverage (eg, the lower extremities) (12).

The most important clinical benefit, however, proved to be the ability to scan a given anatomic volume within a given scan time with substantially reduced section width at *m* times increased longitudinal resolution. Because of this, the goal of isotropic resolution was within reach for many clinical applications. Examinations of the entire thorax (13) or abdomen could now be routinely performed with a 1.0- or 1.25-mm collimated section width. Despite these promising advances, clinical challenges and limitations remained for four-section CT systems. True isotropic resolution for routine applications had not yet been achieved, because the longitudinal resolution of about 1 mm does not fully match the in-plane resolution of about 0.5–0.7 mm in a routine examination of the chest or abdomen. For large volumes, such as for CT angiography of lower extremity vessels (12), thicker (eg, 2.5-mm) collimated sections had to be chosen to complete the scan within a reasonable time frame. Scan times were often too long to allow image acquisition during a purely arterial phase. For CT angiography of the circle of Willis, for instance, a scan range of about 100 mm must be covered (14). With four-section CT at a collimated section width of 1 mm, pitch of 1.5, and gantry rotation time of 0.5 second, this volume can be covered in about 9 seconds, not fast enough to avoid venous overlay, assuming a cerebral circulation time of less than 5 seconds. (Note: The definition of pitch for multi–detector row CT is discussed later in this review.)

As a next step, the introduction of an eight–detector row CT system in 2000 enabled shorter scan times but did not yet provide improved longitudinal resolution (thinnest collimation, eight sections at 1.25 mm). The latter was achieved with the introduction of 16–detector row CT (15), which made possible the routine acquisition of substantial anatomic volumes with isotropic submillimeter spatial resolution and scan times of less than 10 seconds for 300 mm of coverage (Fig 1). While in-plane spatial resolution is not substantially improved, the two major advantages of fast multi–detector row CT are a true isotropic through-plane resolution and a short acquisition time that enable high-quality examinations in severely debilitated and severely dyspneic patients (Fig 1).

Traditional CT applications have been enhanced and strengthened by the remarkable, although incremental, improvement in scanner performance by the addition of more detector rows. Multi–detector row CT also dramatically expanded into areas previously considered beyond the scope of third-generation CT scanners that were based on the mechanical rotation of an x-ray tube and detectors, such as cardiac imaging with the addition of electrocardiographic (ECG)-gating capability. With a gantry rotation time of 0.5 second and dedicated image-reconstruction approaches, the temporal resolution for acquisition of an image was improved to 250 msec and less (16,17), which proved to be sufficient for motion-free imaging of the heart in the mid- to end-diastolic phase when the patient had a slow to moderate heart rate (ie, up to 65 beats per minute [18]). With four simultaneously acquired sections, coverage of the entire heart volume with thin sections (ie, four sections at 1.0- or 1.25-mm collimation) within a single breath hold

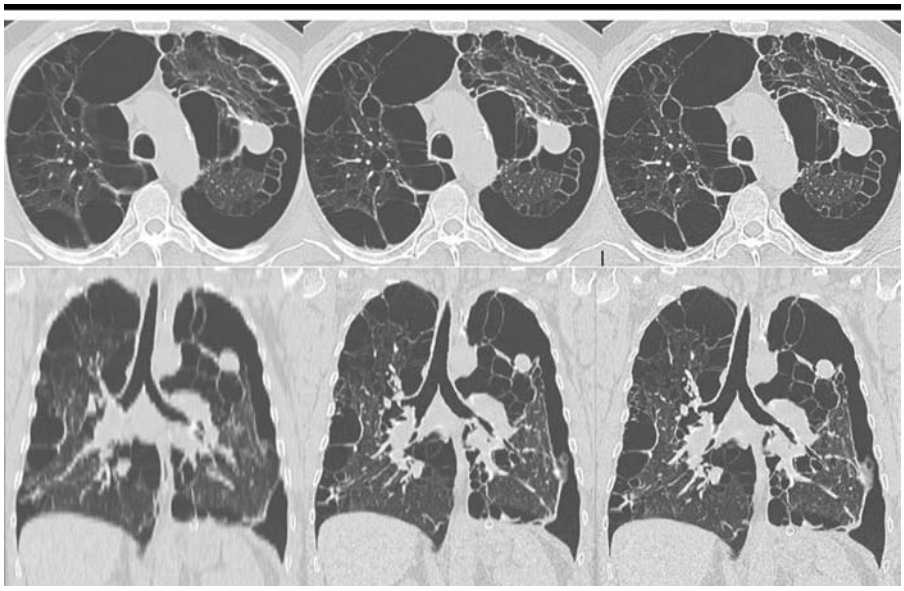

Figure 1. Transverse sections (top) and coronal MPRs (bottom) from a thoracic examination illustrate clinical performance of CT. Left: single-section 8-mm-thick images. Middle: four-section 1.25-mm-thick images. Right: 16–detector row 0.75-mm-thick images. Differences in diagnostic image quality are most obvious in the MPRs. With 16–detector row images, the goal of isotropic resolution in routine examinations has been reached. Single- and four-section images were synthesized from the 16-section CT data.

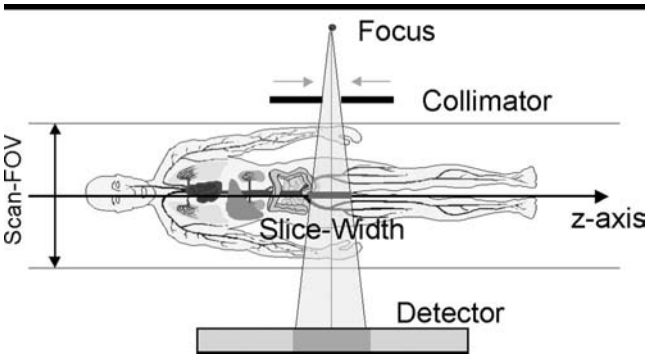

Figure 2. Illustration shows prepatient collimation of the x-ray beam to obtain different collimated section widths with a single–detector row CT detector. *FOV* = field of view.

became feasible. This 1.0–1.25-mm longitudinal resolution combined with the improved contrast resolution of modern CT systems enabled noninvasive depiction of the coronary arteries (19–22). Initial clinical studies demonstrated the potential of multi–detector row CT to not only demonstrate but to some degree also characterize noncalcified and calcified plaques in the coronary arteries on the basis of plaque CT attenuation (22,23).

The limitations of four– and eight–detector row CT systems, however, have so far prevented the successful integration of CT coronary angiography into routine clinical algorithms: Stents or severely calcified arteries constitute a diagnostic dilemma, mainly because of partial volume artifacts as a consequence of insufficient longitudinal resolution (22). For patients with a higher heart rate, careful selection of separate reconstruction intervals for different coronary arteries has been mandatory (25). It is almost impossible for patients with manifest heart disease to comply with the breath-hold time of about 40 seconds required to cover the entire heart volume (approximately 12 cm) with four-section CT. The ongoing technical refinement of multi–detector row CT, however, holds the promise of gradually overcoming some of these limitations. The most important steps toward this goal are gantry rotation times faster than 0.5 second (26,27) for improved temporal resolution and robustness of use, 16-section submillimeter acquisition for increased longitudinal resolution and shorter breath-hold times, and novel sophisticated approaches for image acquisition and reconstruction.

In this review, ECG-synchronized examinations of the heart and of the cardiothoracic anatomy will be very succinctly discussed, since this topic has been extensively reviewed elsewhere (28). Similarly, advanced 3D postprocessing techniques are omitted. In this article, we will review the general technical principles of multi–detector row CT as they apply to the established four– and eight–detector row systems, the more recent 16–detector row scanners, and generations of CT systems yet to come. On the basis of the technologic description of different scanner types and image-reconstruction approaches, we provide practical "take-home points" to enable better translation into daily clinical practice of the technology and science reviewed here. Useful up-to-date information regarding multi–detector row CT is also readily available on the Internet at, for example, the UK Medicines and Healthcare products Regulatory Agency CT Web site *(www.medical-devices.gov.uk)* or the Advanced Medical Imaging Laboratory site *(www.ctisus.org)*.

CURRENT TECHNIQUES

System Design

Detector design.—For clinical purposes, different section widths must be available to adjust the optimum scan speed, longitudinal resolution, and image noise for each application. With a single–detector row CT scanner, different collimated section widths are obtained by means of prepatient collimation of the x-ray beam (Fig 2). For a very elementary model of a two-section CT scanner (m = 2, or two detector rows), Figure 2 demonstrates how different section widths can be obtained by means of prepatient collimation if the detector is separated midway along the z-axis extent of the x-ray beam. For $m > 2$, this simple design principle must be replaced by more flexible concepts requiring more than m detector rows to simultaneously acquire m sections.

Different manufacturers of multi–detector row CT scanners have introduced different detector designs. In order to be able to select different section widths, all scanners combine several detector rows electronically to a smaller number of sec-

tions according to the selected beam collimation and the desired section width.

For established four-section CT systems, two detector types are commonly used. The fixed-array detector consists of detector elements with equal sizes in the longitudinal direction. A representative example of this scanner type, the Lightspeed scanner (GE Medical Systems, Milwaukee, Wis), has 16 detector rows, each of them defining a 1.25-mm collimated section width in the center of rotation (8,10,29). The total coverage in the longitudinal direction is 20 mm at the isocenter; owing to geometric magnification, the actual detector is about twice as wide. By means of prepatient collimation and combination of the signals of the individual detector rows, the following section widths (measured at the isocenter) can be realized: four sections at 1.25 mm, 2.5 mm, 3.75 mm, and 5.0 mm (Fig 3a). The same detector design is used for the eight-section version of this system and provides eight sections at 1.25- and 2.5-mm collimated section widths.

A different approach uses an adaptive-array detector design, which comprises detector rows with different sizes in the longitudinal direction. Scanners of this type, the Mx8000 four-section scanner (Philips Medical Systems, Best, the Netherlands) and the Somatom Sensation 4 scanner (Siemens), have eight detector rows (7,9). Their widths in the longitudinal direction range from 1 to 5 mm at the isocenter and allow the following collimated section widths: two sections at 0.5 mm, four at 1.0 mm, four at 2.5 mm, four at 5.0 mm, two at 8.0 mm, and two at 10.0 mm (Fig 3b).

The selection of the collimated section width determines the intrinsic longitudinal resolution of a scan. In a "step-and-shoot" sequential mode, any multiple of the collimated width of one detector section can be obtained by adding the detector signals during image reconstruction. In a spiral mode, the effective section width, which is usually defined as the full width at half maximum (FWHM) of the spiral section-sensitivity profile (SSP), is adjusted independently in the spiral interpolation process during image reconstruction. Hence, from the same data set, both narrow sections for high-spatial-resolution detail or for 3D postprocessing and wide sections for better contrast resolution or quick review and filming may be derived.

Sixteen-section CT systems usually have adaptive-array detectors. A representative example for this scanner type, the Somatom Sensation 16 scanner (Siemens), uses 24 detector rows (15). The 16 central rows define 0.75-mm collimated section widths at the isocenter, and the four outer rows on both sides define 1.5-mm collimated section widths (Fig 3c). The total coverage in the longitudinal direction is 24 mm at the isocenter. By means of appropriate combination of the signals of the individual detector rows, either 12 or 16 sections with 0.75- or 1.5-mm collimated section width can be acquired simultaneously. The Lightspeed 16 scanner (GE Medical Systems) uses a similar design: It provides 16 sections with either 0.625- or 1.25-mm collimated section width. The total coverage in the longitudinal direction is 20 mm at the isocenter. Yet another design, which is implemented in the Aquilion scanner (Toshiba, Tokyo, Japan), can provide 16 sections with either 0.5-, 1.0-, or 2.0-mm collimated section width, with a total coverage of 32 mm at the isocenter.

Radiation Dose

Radiation dose and dose efficiency.—Radiation exposure to the patient at CT and the resulting potential radiation hazard have recently gained considerable attention in both the public and the scientific literature (30,31). Typical values for the effective patient dose for selected CT protocols are 1–2 mSv for a head CT, 5–7 mSv for a chest CT, and 8–11 mSv for abdominal and pelvic CT (32,33). This radiation exposure must be appreciated in the context of the average annual background radiation, which is 2–5 mSv (3.6 mSv in the United States). Despite the undisputed clinical benefits, multisection CT scanning is often considered to require increased patient dose compared with the dose from single-section CT. Indeed, a certain increase in radiation dose is unavoidable owing to the underlying physical principles.

In the x-ray tube of a CT scanner, a small area on the anode plate, the focal-spot, emits x-rays that penetrate the patient and are registered by the detector. A collimator between the x-ray tube and the patient, the prepatient collimator, is used to shape the beam and to establish the dose profile. In general, the collimated dose profile is a trapezoid in the longitudinal direction. In the umbral region (ie, plateau region of the trapezoid), x-rays emitted from the entire area of the focal spot illuminate the detector. In the penumbral regions, only a part of the focal spot illuminates the detector, while the prepatient collimator blocks off other parts.

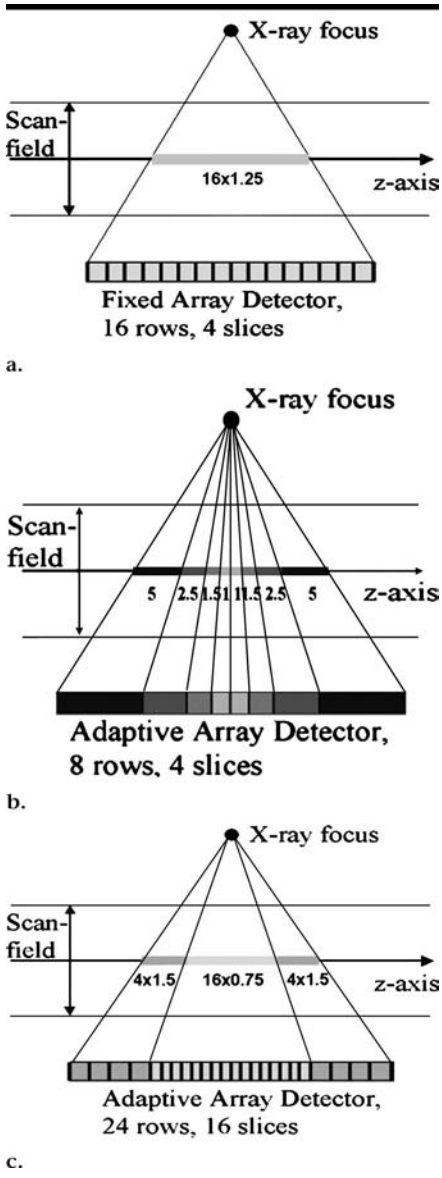

Figure 3. Illustrations show examples of **(a)** fixed-array and **(b, c)** adaptive-array detectors used in commercially available four- and 16-section CT systems.

With single-section CT, the entire trapezoidal dose profile can contribute to the detector signal, and the collimated section width is determined as the FWHM of this trapezoid. The relative dose utilization of a single-section CT system can therefore be close to 100%. In most cases with multi–detector row CT, only the plateau region of the dose profile is used to ensure an equal signal level for all detector elements. The penumbral region is then discarded, either by a postpatient collimator or by the intrinsic self-collimation of the multisection detector, and represents "wasted" dose. The relative contribution of the penumbral region in-

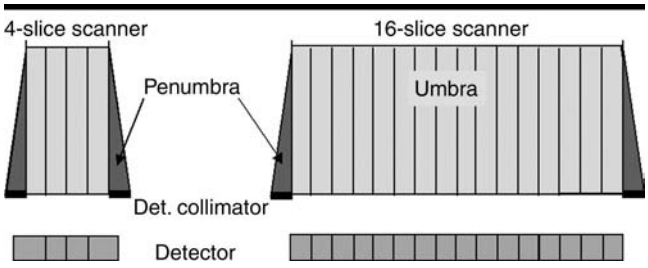

Figure 4. Dose profiles for four- and 16-section CT systems with identical collimated width of one detector *(Det.)* section. The relative contribution of the penumbral region, which represents wasted dose, decreases with increasing number of simultaneously acquired sections.

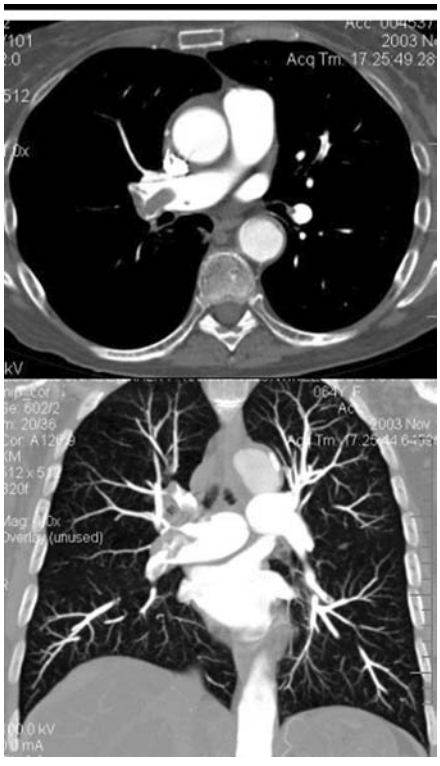

Figure 5. Transverse (top) and coronal maximum intensity projection (bottom; 5-mm slab thickness) thoracic CT images in a patient with pulmonary embolism. Scans were acquired with 16-section scanner at 100 kV and 120 mAs. Effective patient dose was 2.3 mSv, 25% less than for the standard 120 kV protocol. (Images courtesy of Peter Herzog, MD, Klinikum Grosshadern, Munich, Germany.)

creases with decreasing section width, and it decreases with increasing number of simultaneously acquired images. This is demonstrated in Figure 4, which compares the "minimum width" dose profiles for a four-section CT system and a corresponding 16-section CT system with equal collimated width of one detector section. Correspondingly, the relative dose utilization with four-section 1-mm-collimation CT is 70% or less (10), depending on the scanner type. With 16-section CT systems and submillimeter collimation, dose utilization can be improved to 84%, again depending on scanner type (25). Some multi–detector row CT systems offer special implementations of even more dose-efficient modes that use a portion of the penumbral region.

A clinically appropriate measure for dose is the weighted CT dose index, or $CTDI_w$ (34), which uses the absorbed dose in a polymerized methyl methacrylate (acrylic plastic) phantom as an approximation of the dose delivered to a cross section of the patient's anatomy (see Appendix E2, *radiology.rsnajnls.org/cgi/content/full/2353040037/DC1*). Figure E1 (*radiology.rsnajnls.org/cgi/content/full/2353040037DC1*) shows $CTDI_w$ at 120 kV for the 32 cm body phantom as a function of the total collimated width of the detector for a four-section CT system and a 16-section CT system with a similar system geometry. The $CTDI_w$ for 16-section CT at 0.75-mm collimation is 7.8 mGy/100 mAs, whereas the $CTDI_w$ for four-section CT at 1.0-mm collimation is 9 mGy/100 mAs. Thus, different from the transition from single-section CT to 4-section CT systems, a further increase in radiation exposure with the more widespread availability of 16-section CT systems is not to be expected.

Concepts for radiation dose reduction.— The most important factor for reducing radiation exposure is an adaptation of the dose to the patient's size and weight (35–37).

As a general rule for the practicing radiologist, the dose necessary to maintain constant image noise has to be doubled if the patient diameter is increased by 4 cm. Correspondingly, for a patient diameter that is 4 cm smaller than average, half the standard dose is sufficient to maintain adequate image quality. This is of particular importance in pediatric imaging. Dose reduction can be achieved by reductions in the milliampere-seconds and voltage settings. Most CT manufacturers provide dedicated pediatric protocols with, for example, milliampere-seconds and voltage settings adjusted according to the weight of the child.

Another means to reduce radiation dose is to adapt the x-ray tube voltage to the intended application. In contrast agent–enhanced studies such as CT angiography, the contrast-to-noise ratio for fixed patient dose increases with decreasing x-ray tube voltage. As a consequence, to obtain the desired contrast-to-noise ratio, the patient dose can be reduced by choosing a lower voltage setting. The potential for dose saving is more substantial for patients with a smaller diameter. This can be demonstrated, for example, by means of phantom measurements of small tubes filled with diluted contrast agent embedded in acrylic plastic phantoms with different diameters (38). The iodine contrast-to-noise ratio at constant radiation dose for various voltage settings is shown in Figure E2 (*radiology.rsnajnls.org/cgi/content/full/2353040037/DC1*) as a function of the phantom diameter. Compared with a standard scan at 120 kV in a 32-cm-diameter phantom (corresponding to that for an average adult), the same contrast-to-noise ratio is obtained with 0.49 times the dose (1.3 times the milliampere-seconds setting) for 80 kV and 0.69 times the dose (1.1 times the milliampere-seconds) for 100 kV. Thus, ideally, 80 kV should be used for CT angiography in order to reduce patient dose.

Clinical studies (38) have confirmed these findings and demonstrated a potential for dose reduction of about 50% when 80 kV is used for CT angiography instead of 120 kV. In reality, however, the maximum x-ray tube current available at 80 kV is generally not sufficient to scan bigger patients, which limits the routine application of this approach. Therefore, use of 100 kV appears to be a suitable compromise and the method of choice for CT angiography. Figure 5 shows pulmonary CT angiographic images of a patient with pulmonary embolism; the scan was performed on a 16-section scanner at 100 kV and 120 mAs, and the effective patient dose for this scan was 2.3 mSv, 25% less than that for the standard 120-kV protocol. Authors of recent study (39) recommended 100 kV as the standard mode for thoracic and abdominal CT angiography and report dose savings of 30% without loss of diagnostic information.

An approach that is finding increased implementation in clinical practice is anatomic tube current modulation. With this technique, tube output is adapted to the patient geometry during each rotation of the scanner to compensate for strongly varying x-ray attenuation in asymmetric body regions such as the shoulders and pelvis. The variation of the tube output is either predefined by means of an analysis of a localizer scan (topogram, scout view) or is determined online by evaluating the signal from a detector row. With this technique, dose can be reduced by 15%–35% without degrading image quality, depending on the body region (40,41).

In more sophisticated approaches, tube output is modified according to the patient geometry not only during each rotation but also in the longitudinal direction (automatic exposure control), to maintain adequate dose when moving to different body regions (eg, from thorax to abdomen). In one implementation, the attenuation for each body region of a "standard-sized" patient is stored in the control computer. This attenuation corresponds to the milliampere-seconds setting of the standard protocol. If the actual attenuation of the patient deviates from the "standard" attenuation, the tube output is adapted correspondingly. Figure 6 shows the variation of the milliampere-seconds output for a CT scan of the chest and abdomen in a 6-year-old child. Although the standard protocol with 165 mAs was used—which would have resulted in substantially higher radiation dose than necessary in a standard mode of operation—the average milliampere-seconds value throughout the scan was adjusted to 38 mAs by means of automatic exposure control. Automatic adaptation of tube current to patient size prevents both over- and underirradiation, considerably simplifies the clinical workflow for the technician, and eliminates the need for look-up tables of patient weight and size for adjusting the milliampere-seconds settings.

Radiation dose for ECG-synchronized CT for cardiac applications has been a topic of considerable controversy. Recent studies (32,33) based on four-section CT systems find an effective patient dose of roughly 1 mSv for ECG-triggered calcium scoring with 3-mm section width and roughly 10 mSv for ECG-gated CT angiography of the coronary arteries with 1.0- or 1.25-mm section width. Radiation dose in ECG-gated spiral CT can be reduced by 30%–50% with use of ECG-controlled dose modulation (42,43). During the spiral scan, the output of the x-ray tube is modulated according to the patient's ECG trace. It is kept at its nominal value during a user-defined phase of the cardiac cycle—in general, the mid- to end-diastolic phase. During the rest of the cardiac cycle, the tube output is typically reduced to 20% of the nominal values, although it is not switched off entirely, to allow image reconstruction throughout the entire cardiac cycle. Thus, although the signal-to-noise ratio is decreased at certain phases of the cardiac cycle, the low-dose images are still sufficient for evaluation of functional parameters such as ejection fraction, should this kind of information be desired.

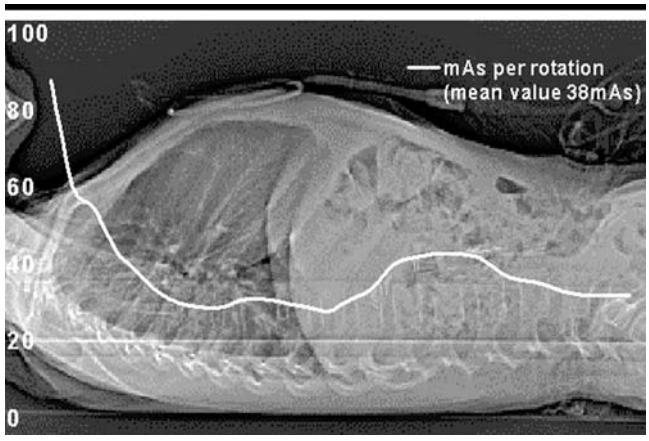

Figure 6. Automatic exposure control. Lateral topogram (scout view) for thoracoabdominal CT in a 6-year-old child is shown with automatically adapted milliampere-seconds value as function (curve) of z-axis position during spiral CT. Although the standard adult protocol with 165 mAs was used, the average milliampere-seconds value throughout the scan was adjusted to 38 mAs owing to automatic exposure control. (Image courtesy of Michael Lell, MD, University of Erlangen, Germany.)

SEQUENTIAL SCANS AND IMAGE-RECONSTRUCTION TECHNIQUES

With the advent of multi–detector row CT, sequential "step-and-shoot" scanning has remained in use for only a few clinical applications, such as head CT, high-spatial-resolution lung CT, perfusion CT, and interventional applications. A detailed theoretical description to predict the performance of multi–detector row CT in sequential mode can be found in reference 44.

The number of images acquired during a sequential scan corresponds to the number of active detector sections. By adding the detector signals of the individual sections during image reconstruction, the number of images per scan can be reduced, and the image section width can be increased. As an example, a scan with four sections at 1.0-mm collimation provides either four images with 1.0-mm section width, two images with 2.0-mm section width, or one image with 4.0-mm section width.

The option to realize a wider section by summing several thin sections is beneficial for examinations that require narrow collimation to prevent partial volume artifacts and low image noise to allow detection of low-contrast details (eg, neurologic examinations of posterior fossa or cervical spine). In the head, partial volume artifacts typically manifest as dark streaks or areas of hypoattenuation and are due to a nonlinear effect that has been described in reference 45. Figure 7 shows an example of a patient who underwent follow-up CT after surgical removal of a pituitary tumor. From the same scan data—four sections at 1.0-mm collimation—both 4.0-mm-thick images with a standard head kernel for soft-tissue evaluation and 1.0-mm-thick images with a bone kernel were reconstructed. For best image quality, the posterior fossa should be scanned with a collimated section width not larger than 1.25 mm, whereas wider collimation can be used in the supratentorial region (46).

SPIRAL SCANS AND IMAGE-RECONSTRUCTION TECHNIQUES

Spiral scanning is the method of choice for the majority of all multi–detector row CT examinations and requires more at-

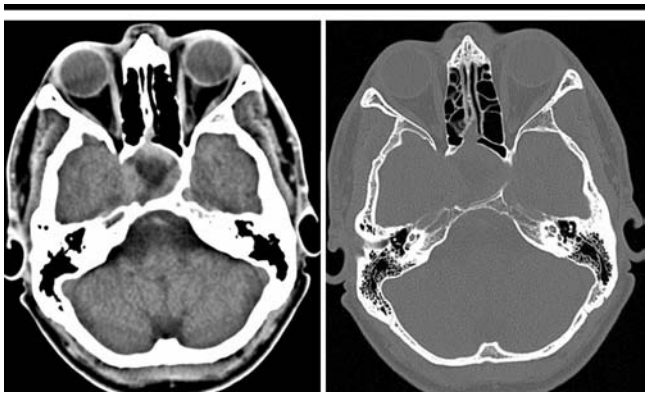

Figure 7. Clinical performance of four-section CT in sequential scan mode. Follow-up images in a patient after surgical removal of pituitary tumor. Left: 4-mm-thick image with standard head kernel for soft-tissue evaluation. Right: 1-mm-thick image with bone kernel for bone evaluation. Both images were generated from the same scan data (four sections at 1-mm collimation).

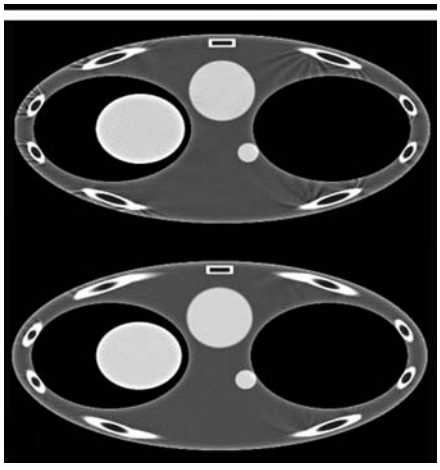

Figure 8. Transverse sections of anthropomorphic thorax phantom from 16-section CT at 0.75-mm collimation and pitch of 1. Images were reconstructed with adaptive multiplanar reconstruction (AMPR; Siemens), with 1.0-mm (top) and 3.0-mm (bottom) section width. Spiral interpolation artifacts are reduced with sections widths that are thick relative to collimation. In clinical practice, best image quality for a desired section width is obtained by acquiring narrow-collimation data.

tention than does sequential multi–detector row CT because it is conceptually more demanding.

Definition of Spiral Pitch

An important parameter for characterizing a spiral CT scan is the pitch. According to International Electrotechnical Commission specifications (34), the pitch *(p)* is given by $p = TF/W$, where TF is the table feed per rotation, and W is the total width of the collimated beam. This definition holds for both single-section and multi–detector row CT. It shows whether data acquisition occurs with gaps ($p > 1$) or with overlap ($p < 1$) in the longitudinal direction. With 16 sections at 0.75-mm collimation and a table-feed of 18 mm per rotation, the pitch is $p = 18/(16 \times 0.75) = 18/12 = 1.5$. With four sections at 1.0-mm collimation and a table-feed of 6 mm per rotation, the pitch again is $p = 6/(4 \times 1) = 6/4 = 1.5$. In the early days of four-section CT, the term *detector pitch* had been additionally introduced, which accounts for the width of a single section in the denominator. For the sake of clarity and uniformity, the detector pitch should no longer be used.

Short Review of Single-Section Spiral CT Reconstruction

Spiral CT requires an interpolation of the acquired measurement data in the longitudinal (through-plane) direction to estimate a complete CT data set at the desired plane of reconstruction. The most commonly used single-section spiral interpolation schemes are the 360° and 180° linear interpolation methods.

The 360° linear interpolation method exploits the 360° periodicity of the projection data (1,2). For each projection angle, a linear interpolation is performed between those two projections on either side of the image plane that are positioned closest to the image plane and are 360° apart (ie, are measured in subsequent rotations). The 180° linear interpolation technique makes use of the fact that for each measurement ray, an interpolation partner is already available after approximately half a rotation (47), when the x-ray tube and detector have exchanged positions. This is the so-called complementary ray. In spiral CT, z-axis resolution is determined not only by the collimated beam width (as in sequential scanning) but also by the effective section width, which is established in the spiral interpolation process. Usually, the effective section width is defined as the FWHM of the SSP. Effective section width increases with increasing pitch for both 360° and 180° linear interpolation, and longitudinal resolution degrades (Fig E3, *radiology.rsnajnls.org/cgi/content/full/2353040037/DC1*). This is a consequence of the increasing longitudinal distance of the projections used for spiral interpolation. With 180° linear interpolation, the effective sections width equals the collimated section width at a pitch of 1, but effective section width equals 1.27 times the collimated width at a pitch of 2, so that a collimated 5-mm-thick section is an actual 6.4-mm-thick section at a pitch of 2. The image noise in single-section spiral CT is independent of the pitch if the tube current (in milliamperes) is left unchanged, and patient dose decreases with increasing pitch (see Appendix E2, *radiology.rsnajnls.org/cgi/content/full/2353040037/DC1*).

Single-section spiral CT is based almost exclusively on 180° linear interpolation, owing to the narrower SSP of this algorithm, despite its increased susceptibility to artifacts and increased image noise. For the same milliampere-seconds setting, image noise is about 15% higher than that in sequential CT mode. Spiral artifacts gradually increase as pitch is increased. Spiral artifacts typically manifest as hyper- or hypoattenuating "windmill" structures surrounding z-axis inhomogeneous high-contrast objects (eg, bones), which rotate when scrolling through a stack of images. Spiral artifacts are caused by the spiral interpolation process and can also be observed on multi–detector row CT images (see Fig 8). With single-section CT, scanning at a higher pitch is often used to reduce patient dose at the expense of section broadening—if the collimation is kept constant—and increased spiral artifacts. For CT angiographic applications in particular, it is more favorable to scan a given volume in a given time by using narrow collimation at a high pitch rather than wider collimation at a low pitch. The motivation for increasing pitch and reducing collimation is to improve longitudinal resolution by narrowing the SSP (48).

The Cone-Angle Problem in Multi–Detector Row CT

Two-dimensional image-reconstruction approaches used in commercially available single-section CT scanners require all measurement rays that contribute to an image to run in a plane perpendicular to the patient's longitudinal axis. In multi–detector row CT systems, this requirement is violated. Figure 9 shows the geometry of a four-section scanner: The measurement rays are tilted by the so-called cone angle with respect to the center plane. The cone angle is largest for the sections at the outer edges of the detector, and it increases as the number of detector rows increases, if their width is kept constant. As a first approximation, the cone angle is neglected in multi–detector row CT reconstruction approaches: The measurement rays are treated as if they traveled perpendicular to the z-axis, and modified two-dimensional image-reconstruction algorithms are used. The data are then inconsistent, however, and produce cone-beam artifacts at high-contrast objects such as bones. It has been demonstrated that cone-beam artifacts can be tolerated if the maximum number of simultaneously acquired sections does not markedly exceed four (49). As a consequence, the image-reconstruction approaches of all commercially available four-section CT systems and of some systems with even more sections neglect the cone angle of the measurement rays.

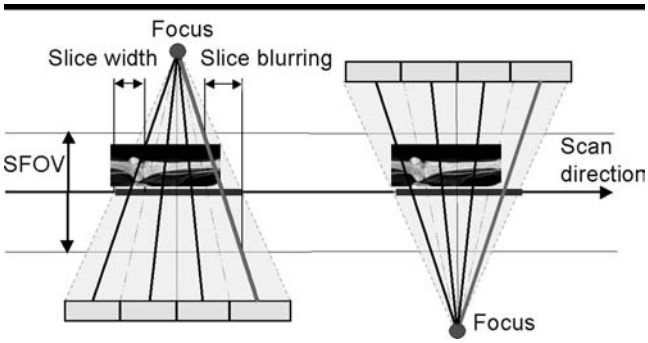

Figure 9. Diagram shows geometry of four-section CT scanner demonstrating the cone-angle problem: Measurement rays are tilted by the so-called cone angle with respect to the center plane. Left and right: Two view angles from sequential scan that are shifted by 180° so that positions of x-ray tube and detector are interchanged. With single-section CT, identical measurement values would be acquired. With multi–detector row CT, different measurement values are acquired. *SFOV* = scan field of view.

MULTI–DETECTOR ROW SPIRAL CT RECONSTRUCTION APPROACHES THAT NEGLECT CONE-BEAM GEOMETRY

Multi–Detector Row 180° and 360° Linear Interpolation

The 360° and 180° linear interpolation single-section spiral reconstruction approaches can be extended to multi–detector row spiral scanning in a straightforward way (29,50,51). Both 360° and 180° multidetector linear interpolation methods are characterized by a projection-wise linear interpolation between two rays on either side of the image plane. The cone angle of the measurement rays is not taken into account. In the 360° linear interpolation spiral reconstruction approach, rays measured either at the same projection angle by different detector rows or in consecutive rotations of the scanner (ie, 360° apart) are used for spiral interpolation. In the 180° spiral reconstruction approach, both direct and complementary rays are considered. At the isocenter, direct and complementary rays interleave in the z-axis direction for selected pitch values. This way, the distance between measured samples is substantially reduced and equals half the collimated section width, which results in the desired narrow SSPs. Appropriate pitch values are 0.75 for four-section scanning (29) and 0.5625 or 0.9375 for 16-section scanning (50). The 180° and 360° multidetector linear interpolation approaches are schematically illustrated in Figure E4 (*radiology.rsnajnls.org/cgi/content/full/2353040037/DC1*) for the example of a four-section CT scanner.

In general, scanners that rely on 180° or 360° multidetector linear interpolation techniques and extensions thereof provide selected discrete pitch values to the user, such as 0.75 and 1.5 for four-section scanning (29) or 0.5625, 0.9375, 1.375, and 1.75 for 16-section scanning (50). These pitch values are intended to provide optimized sampling schemes in the longitudinal direction and, hence, optimized image quality.

The user has to be aware of pitch-dependent effective section widths. For low-pitch scanning (pitch of 0.75 for four sections and 0.5625 or 0.9375 for 16 sections), the effective section width approximates the collimated section width; for a 1.25-mm collimated section width, the resulting effective section width remains 1.25 mm. The narrow SSP, however, is achieved by using 180° multidetector linear interpolation reconstruction with conjugate interpolation at the price of increased image noise (29,50). For high-pitch scanning (pitch of 1.5 for four sections and 1.375 or 1.75 for 16 sections), the effective section width is approximately 1.27 times the collimated section width, and a 1.25-mm collimated section width results in a 1.5–1.6-mm effective section width.

When comparing dose and image noise for different pitch values, the widening of the SSP has to be taken into account. To obtain the same image noise as in a sequential scan with the same collimated section width, 0.73–1.68 times the dose (depending on spiral pitch) is required, with the lowest dose at the highest pitch (see reference 50). Some manufacturers provide a semiautomatic adaptation of the milliampere value to keep the image noise constant if the pitch is changed. In clinical practice, therefore, it is permissible to assume that scanners offering discrete optimized pitch values based on 180° and 360° multidetector linear interpolation techniques are comparable to single-section CT systems in some core aspects: At high pitch, the section widens and the longitudinal resolution degrades; at low pitch, the narrowest possible SSP (comparable to that of 180° single-section linear interpolation at pitch of 1) can be obtained, but a higher dose is necessary to maintain the signal-to-noise ratio. Thus, as a take-home point, when one selects the scan protocol for a particular application, scanning at low pitch optimizes image quality and longitudinal resolution at a given collimation but at the expense of increased patient dose. To reduce patient dose, either milliampere settings should be reduced at low pitch values or high pitch values should be chosen.

Z-Filter Approaches

In a z-filter multi–detector row spiral reconstruction (51,52), the spiral interpo-

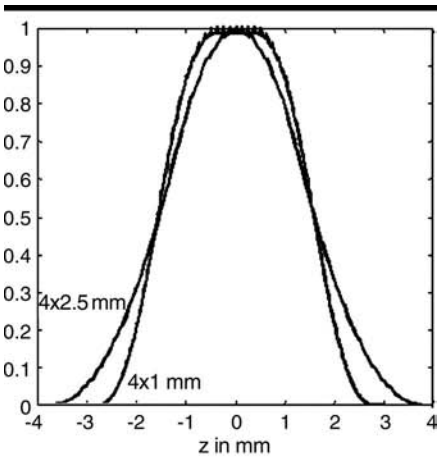

a.

b.

Figure 10. **(a)** SSP of 3-mm section for four-section CT at 1.0- and 2.5-mm collimation. **(b)** Images of thorax phantom with 3.0-mm section width obtained from four-section CT at 2.5 mm collimation and pitch of 0.75 (top) and at 1.0-mm collimation and pitch of 1.75 (bottom). Despite higher pitch, image acquired with 1.0-mm collimation shows reduced artifacts at ribs.

lation for each projection angle is no longer restricted to the two rays closest to the image plane. Instead, all direct and complementary rays within a selectable distance from the image plane contribute to the image. The weighting function for the rays is selectable, which allows one to adjust both the functional form and the FWHM of the spiral SSP. Still, the cone angle is neglected. A representative example of a z-filter approach is the adaptive axial interpolation algorithm (51) implemented in Siemens CT scanners, which is illustrated in Figure E5 (*radiology.rsnajnls.org/cgi/content/full/2353040037/DC1*). Another example is the "multislice cone-beam tomography," or MUSCOT, algorithm (52) used by Toshiba. Z filtering allows the system to trade off z-axis resolution (the SSP) with image noise (which directly correlates with required dose).

With adaptive axial interpolation, the spiral pitch is freely selectable in the range 0.5–2.0, and the same effective section width, which is defined as the FWHM of the spiral SSP, is generated at all pitch values (7,51,53). Therefore, longitudinal resolution is independent of pitch, unlike single-section spiral CT and multi–detector row CT that relies on 180° and 360° linear interpolation (51,54). Figure E6 (*radiology.rsnajnls.org/cgi/content/full/2353040037/DC1*) shows the SSPs of a 2-mm section (for four-section CT at 1-mm collimation) and MPRs of a spiral z-axis resolution phantom for selected pitch values. As a consequence of the pitch-independent spiral section width, the image noise for a fixed tube current (in milliamperes) would decrease as pitch is decreased, owing to the increasingly overlapping spiral acquisition. Instead, the user selects an "effective" milliampere-seconds value, and the tube current is then automatically adapted to the pitch of the spiral scan to compensate for dose accumulation. The dose for fixed effective milliampere-seconds is independent of the spiral pitch and equals the dose of a transverse scan with the same milliampere-seconds setting (see Appendix E2, *radiology.rsnajnls.org/cgi/content/full/2353040037/DC1*).

Thus, as a take-home point, unlike in single-section spiral CT a change in pitch does not result in a change in dose to the patient. Accordingly, the use of a higher pitch does not result in a dose saving, which is an important practical consideration with CT systems that rely on adaptive axial interpolation.

The intrinsic resolution of a multi–detector row spiral scan is determined by the choice of collimation (eg, four sections at 1.0 or 2.5 mm). Z filtering makes it possible to reconstruct images retrospectively with different section widths from the same raw CT data set. Only section widths equal to or larger than the section width of one active detector row can be obtained. In many cases, both thick sections for initial viewing and recording and thin sections for detailed diagnosis or as an input for advanced 3D postprocessing are routinely reconstructed.

The thinnest available section width is the collimated section width (1.0 mm for four sections at 1.0-mm collimation), which is created by using nonlinear spiral weighting functions at the expense of increased image noise and increased susceptibility to artifacts. Thus, as a take-home point, the thinnest available section should only be used for high-contrast applications such as high-spatial-resolution lung imaging. For general purpose scanning, a 1.25-mm section width for four-section CT at 1.0-mm collimation (and 3.0-mm section width for four sections at 2.5-mm collimation) is recommended as the most suitable trade-off between longitudinal resolution, image noise, and artifacts, in particular when thin sections are reconstructed as an input for 3D postprocessing such as for MPR, maximum intensity projection, or volume-rendering techniques. For a 1.25-mm spiral section width reconstructed from four-section CT at 1.0-mm collimation, 0.61–0.69 times the dose (depending only slightly on spiral pitch) is required to maintain the image noise of a sequential scan at the same collimation (see references 54,55). Unlike 180° and 360° multidetector linear interpolation, image noise is therefore practically independent of pitch at constant dose.

For a given collimation, such as four sections at 2.5 mm, image quality can be optimized with regard to spiral artifacts by lowering the pitch (56). Another means to reduce spiral artifacts is to use narrow collimation: A given section width (eg, 3.0 mm) can be obtained with different collimations, in this case four sections at 1.0 mm and at 2.5 mm. For optimum image quality, collimation that is narrow relative to the desired section width is preferable (51). Furthermore, a more rectangular SSP can be established. Figure 10a shows the SSPs of a 3.0-mm section for four-section CT at both 1.0- and 2.5-mm collimation. Figure 10b shows 3.0-mm transverse sections of a thorax phantom scanned with four-section CT at 2.5- and 1.0-mm collimation. Despite the higher pitch, the 3.0-mm image obtained at 1.0-mm collimation shows fewer artifacts. Similar to single-section spiral CT, narrow collimation at

high pitch is preferable to wide collimation at low pitch for artifact reduction.

Except for a minor dose increase due to the different relative contributions of the penumbral zones of the dose profile, scanning at narrow collimation does not result in higher radiation dose to the patient as long as the effective milliampere-seconds level is kept constant. Narrow-collimation scanning should, therefore, be the protocol of choice for all applications that require 3D postprocessing as part of the clinical evaluation. In the clinical treatment of uncooperative or trauma patients or for protocols such as routine oncologic staging, the use of wider collimation can be considered. The best suppression of spiral artifacts is achieved by using both narrow collimation (relative to the desired section width) and reduced spiral pitch.

In general, more challenging clinical protocols, such as CT of the spine and of the skull base, are reliant on a combination of narrow collimation and low pitch. When multi–detector row spiral CT of the head is performed with narrow collimation, low pitch, and z-filter reconstruction of wider sections, the results are equivalent to those of traditional sequential CT. Figure 11 shows an example of a head scan performed with a four-section CT system in which a sequential image (two-section CT at 8 mm) and a spiral image (8-mm section width from four-section CT at 1-mm collimation) are compared in the same patient.

Some manufacturers who use a z-filter approach do not provide completely free selection of the spiral pitch but recommend a selection of fixed pitch values (eg, pitch of 0.625, 0.75, 0.875, 1.125, 1.25, 1.375 and 1.5 for four-section CT with the MUSCOT algorithm [52]) that are aimed at optimizing the z-axis sampling scheme and reducing spiral artifacts.

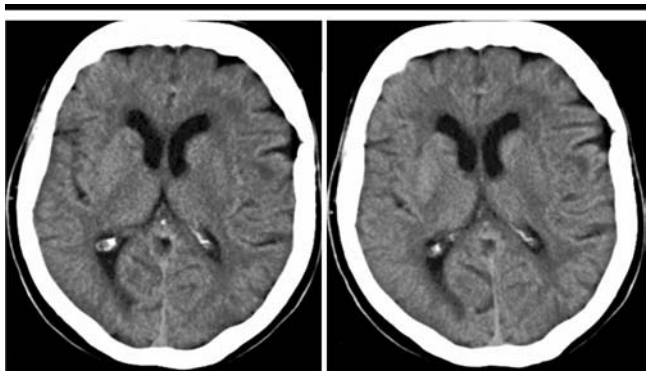

Figure 11. Transverse head examination performed with four-section CT system. Comparison of sequential image obtained at two-section CT at 8.00-mm section width (left) and spiral image (right; 8.0-mm section width from four-section CT at 1.0-mm collimation) in same patient. Image quality can be considered equivalent owing to narrow-collimation z-filter reconstruction. (Image courtesy of Roland Brüning, MD, Klinikum Grosshadern, Munich, Germany.)

MULTI–DETECTOR ROW SPIRAL RECONSTRUCTION APPROACHES THAT ACCOUNT FOR CONE-BEAM GEOMETRY

Overview of Cone-Beam Reconstruction Algorithms

For CT scanners with 16 or more detector rows, modified reconstruction approaches that account for the cone-beam geometry of the measurement rays have to be considered. Some manufacturers (Toshiba, Philips) have extended the Feldkamp algorithm (57,58), an approximate 3D convolution back-projection reconstruction that was originally introduced for sequential scanning, to multisection spiral scanning (59,60). With this approach, the measurement rays are back projected into a 3D volume along the lines of measurement, accounting in this way for their cone-beam geometry. Three-dimensional back projection is computationally demanding and requires dedicated hardware to achieve acceptable image-reconstruction times. Other manufacturers use variations and extensions of nutating-section algorithms (61–66) for image reconstruction. These algorithms split the 3D reconstruction task into a series of conventional two-dimensional reconstructions on tilted intermediate image planes, in this way benefiting from established and very fast two-dimensional reconstruction techniques. Representative examples are AMPR (Siemens) (67,68) and the weighted hyperplane reconstruction (proposed by GE Medical Systems) (69,70) techniques.

AMPR Method

The AMPR approach (67,68) is an extension and generalization of the "advanced single-slice rebinning" (63,64) method. AMPR allows free selection of the spiral pitch with optimized dose utilization, which is beneficial for medical applications. With advanced single-slice rebinning, a partial scan interval (about 240° of scan data) is used for image reconstruction. The image planes are no longer perpendicular to the patient axis; instead, they are tilted to match the spiral path of the focal spot; see Figure 12 for a 16-section scanner at a pitch of 1.5. For every view angle in this partial scan interval, the focal spot is positioned in or near the image plane—that is, measurement rays running in or very close to the image plane are available. These conditions need to be fulfilled for a standard two-dimensional reconstruction. In a final z-axis reformation step, the traditional transverse images are calculated by interpolating between the tilted original image planes.

Advanced single-slice rebinning encounters its limitations when the spiral pitch is reduced to make use of the overlapping spiral acquisition and the resulting dose accumulation. The AMPR algorithm (67,68) addresses this problem: Instead of all available data being used for a single image, the data are distributed to several partial images on double-oblique image planes, which are individually adapted to the spiral path and fan out like the pages of a book (Fig 13, left). To ensure full dose utilization the number of partial images ("pages" in the book), as well as the length of the data interval per image, depend on the spiral pitch. The final transverse (or arbitrarily oriented) images are calculated by means of z-axis interpolation between the tilted partial image planes (Fig 13, right). The shape and the width of the z-axis interpolation functions are selectable. Different SSPs and different section widths can therefore be adjusted, so that z-axis resolution (SSP) can be traded off with image noise. The spiral pitch is freely selectable and the section width—and consequently the z-axis resolution—are independent of the pitch. The concept of effective milliampere-seconds and automatic adaptation of the tube current to the pitch also apply to

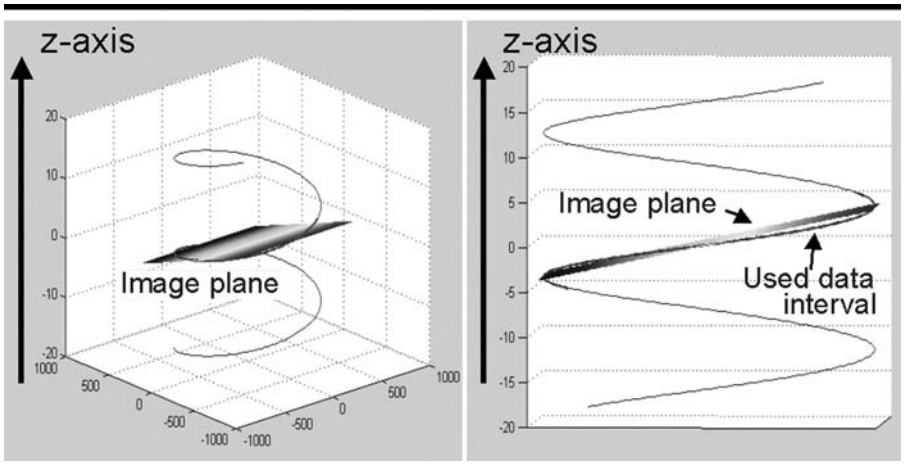

Figure 12. Left: Schematic 3D illustration of "advanced single-slice rebinning" approach for 16-section CT system at pitch of 1.5. Left: Curved line represents spiral path of the focal spot. Intermediate image plane is indicated by gradient-shaded rectangle and is no longer perpendicular to patient axis; instead, it is tilted to match spiral path of the focal spot. Right: Projection onto a plane containing the z-axis, where the spiral path is represented as a sinusoidal line. A partial scan interval (about 240°) is used for image reconstruction. For all view angles, focal spot is close to the image plane.

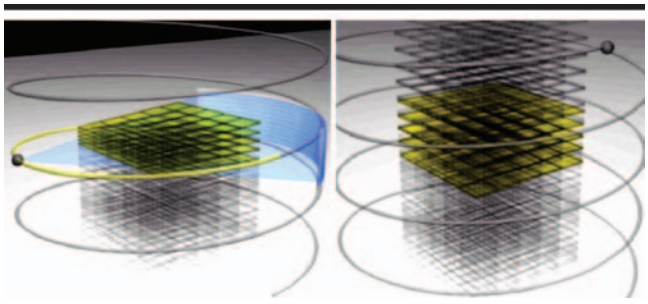

Figure 13. Illustration of AMPR approach. Left: First, multisection spiral CT data are used to reconstruct several partial images on double-oblique image planes, which are individually adapted to the spiral path. Partial images fan out like pages of a book. Right: Second, final images with full dose utilization are calculated with z-axis interpolation between tilted partial image planes.

AMPR (see Appendix E2, *radiology.rsnajnls.org/cgi/content/full/2353040037/DC1*).

With the AMPR approach, sufficient image quality is obtained for all pitch values between 0.5 and 1.5 (68). Figure 14 shows transverse sections and MPRs of an anthropomorphic thorax phantom. Scan data for 16 sections at 0.75-mm collimation and pitch of 1 were reconstructed with 1-mm section width with z filtering, the AMPR algorithm, and 3D back projection. Neglecting the cone angle leads to artifacts at high-contrast objects and geometric distortions, particularly in MPRs (Fig 14, top). Both AMPR and 3D back projection restore the spatial integrity of the high-contrast objects, reduce cone-beam artifacts, and are fully equivalent for 16-section scanning. Recent studies have demonstrated the adequacy of extended versions of AMPR for medical CT systems with up to 64 detector rows (71).

The remaining artifacts in Figure 14 are spiral interpolation artifacts (windmill artifacts), not cone-beam artifacts. Windmill artifacts are not related to the cone-beam geometry and result from the finite width of the detector rows, which require interpolation between the rows for image reconstruction. Hence, windmill artifacts occur independent of the reconstruction approach. They are exaggerated in the mathematic phantom shown (Fig 14) and can be reduced by decreasing the pitch and/or increasing the reconstruction section width relative to the collimation (Fig 8). Figure 15 shows MPRs of a z-axis resolution phantom scanned with 16-section CT at 0.75-mm collimation and pitches of 0.75, 1.0, 1.25, and 1.5. Independent of the pitch, all cylinders down to 0.6 mm in diameter can be resolved, the MPRs are relatively free of geometric distortions, and the spatial integrity of the 3D image is maintained.

Multi–detector row spiral CT with AMPR is characterized by the same key properties as adaptive axial interpolation, which can be directly derived from information in the section on z-filter reconstruction presented earlier in this review. Thus, all recommendations regarding selection of collimation and pitch that were discussed there also apply for AMPR. In particular, a change in pitch does not result in a change in radiation exposure to the patient, and the use of higher pitch does not result in dose saving. Narrow collimation should be used whenever possible. With 16-section 0.75-mm-collimation CT, the thinnest available reconstruction section width of 0.75 mm is created by using nonlinear weighting functions at the z-axis image-reformation step, at the expense of increased image noise and increased susceptibility to artifacts. As a take-home point, this approach again should only be used for high-contrast applications such as high-spatial-resolution lung imaging. When thin sections are reconstructed as input for 3D postprocessing such as MPR, maximum intensity projection, or volume-rendering techniques, a 1.0-mm section width is recommended as the most suitable trade-off between longitudinal resolution, image noise, and artifacts.

Weighted Hyperplane Reconstruction

The weighted hyperplane reconstruction method, which has been described elsewhere (69,70), uses concepts related to AMPR but is derived differently. Similar to AMPR, 3D reconstruction is split into a series of two-dimensional reconstructions. Instead of reconstruction of traditional transverse sections, convex hyperplanes are proposed as the region of reconstruction. The increasing spiral overlap with decreasing pitch is handled by introducing subsets of detector rows, which are sufficient to reconstruct an image at a given pitch value. At pitch of 0.5625 with a 16-section scanner, the data collected by detector rows one to nine form a complete projection data set. Similarly, projections from detector rows two to 10 can be used to reconstruct another image at the same z-axis position. Projections from detector rows three to 11 yield a third image and so on. In a way, these "subimages" are related to the "book pages" of AMPR. The final image is

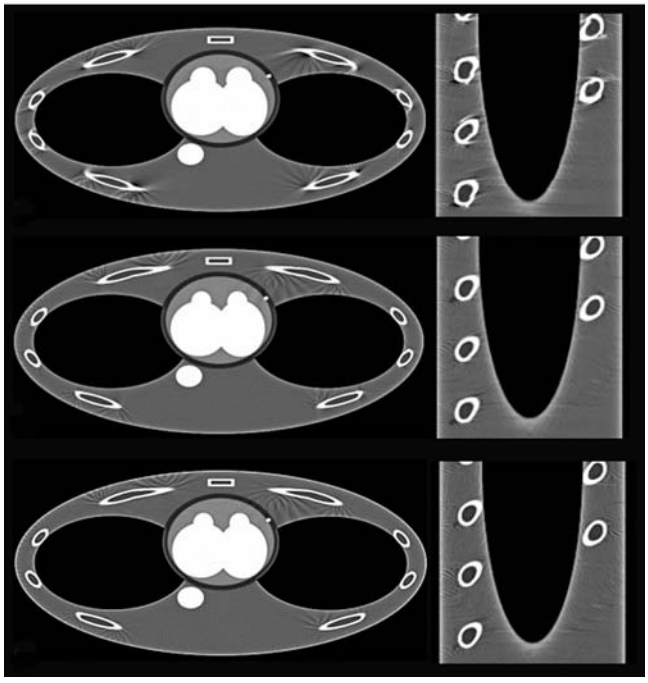

Figure 14. Transverse sections (left) and sagittal MPRs (right) of anthropomorphic thorax phantom. Scan data for 16-section CT at 0.75-mm collimation and pitch of 1 were reconstructed with 1.0-mm section width and z filtering that neglected the cone angle of measurement rays (top), with AMPR algorithm (middle), and with 3D back projection (bottom). Neglecting cone angle leads to artifacts at high-contrast objects, particularly in MPRs (top). Both AMPR (middle) and 3D back-projection (bottom) images reduce cone-beam artifacts and are fully equivalent for 16-section CT.

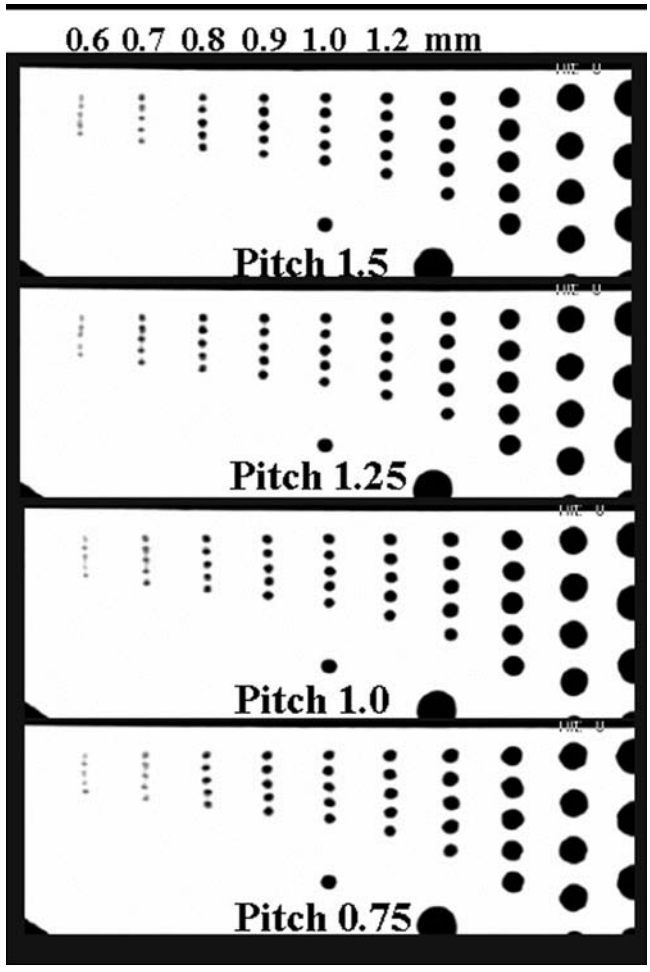

Figure 15. MPRs of z-axis resolution phantom at isocenter, scanned with 16-section CT at 0.75-mm collimation and pitches of 1.5, 1.25, 1.0, and 0.75 (MPR section width, 0.75 mm; increment, 0.4 mm). Phantom consists of polymerized methyl methacrylate plate with rows of cylindrical holes (diameters of 0.5, 0.6, 0.7, 0.8, 0.9, 1.0, 1.2, 1.5, 2.0, and 3.0 mm) aligned in the longitudinal direction. Independent of pitch, all cylinders down to 0.6 mm in diameter can be resolved.

based on a weighted average of the subimages. In the article by Hsieh et al (70), good image quality was demonstrated for a 16-section CT system (Lightspeed 16; GE Medical Systems) with which the weighted hyperplane reconstruction approach was used. By performing parameter optimizations, an optimal balance among various system performance parameters, such as noise, artifacts, and SSPs, can be achieved (72).

ECG-SYNCHRONIZED SCAN AND IMAGE-RECONSTRUCTION TECHNIQUES

One of the most exciting new applications of multi–detector row CT is the ability to image the heart and the cardiothoracic anatomy without motion artifacts. For ECG-synchronized scanning of the cardiothoracic anatomy, either ECG-triggered sequential scanning or ECG-gated spiral scanning can be used. In ECG-triggered sequential scanning, the heart volume is covered by subsequent transverse scans with a step-and-shoot technique. For each transverse scan, the number of images corresponds to the number of active detector sections. A partial scan data interval is acquired with a predefined temporal offset relative to the R waves of the patient's ECG trace, which can be either relative (as a certain percentage of the R-R interval) or absolute (in milliseconds) and either forward or reverse (17). Some 16-section CT systems offer gantry rotation times shorter than 0.5 second (eg, 0.42, 0.40, or 0.37 second). In this case, temporal resolution can be as good as 0.21, 0.20, or 0.185 second (26,27).

With retrospective ECG gating, the heart volume is covered continuously by a spiral scan. The basic concepts for ECG-gated spiral imaging, such as single-segment and multisegment reconstruction, had already been developed in 1998 (73). The patient's ECG signal is recorded at the same time the CT data are acquired to allow retrospective selection of the data segments used for image reconstruction. Only scan data acquired in a predefined cardiac phase, usually the diastolic phase, are used for image reconstruction (16,17,74,75). The data segments contributing to an image begin with a user-defined offset relative to the onset of the R waves, similar to ECG-triggered sequential scanning. Image reconstruction generally consists of two steps: multi–detector row spiral interpolation to compensate for the continuous table movement and to obtain scan data at the desired image z-axis position, followed by a partial scan reconstruction of the transverse data segments. The temporal resolution of an image can be improved up to $t_{rot}/(2N)$ by using scan data of N subsequent heart cycles for image formation in a so-called multisegment recon-

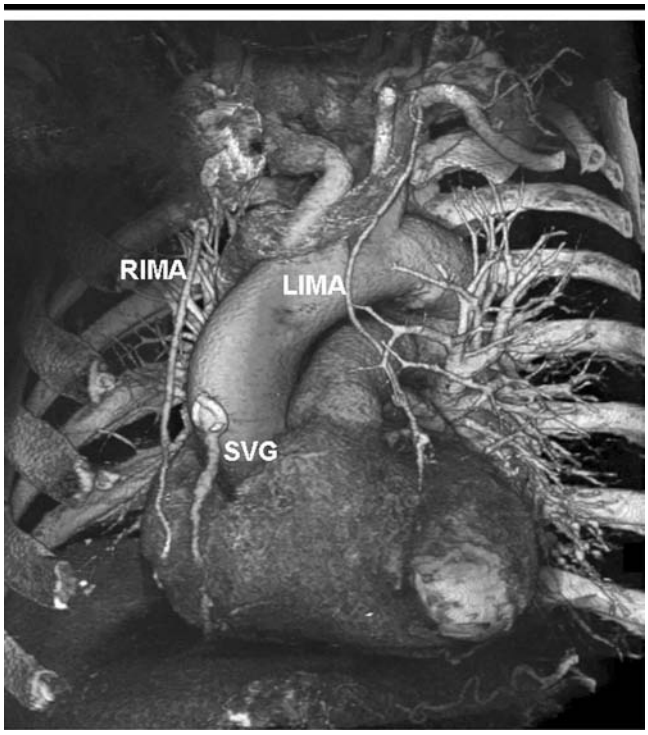

Figure 16. Clinical performance of ECG-gated 16-section CT (0.75-mm collimation, 0.42-second gantry rotation) of entire thorax. Coronal volume-rendered reconstruction shows left internal mammary bypass graft *(LIMA)* to left anterior descending coronary artery and saphenous venous bypass graft *(SVG)* to right coronary artery. Native right internal mammary artery *(RIMA)* is also visible.

struction mode (16,73–77), where t_{rot} is the gantry rotation time of the CT scanner. With increased *N,* better temporal resolution is achieved but at the expense of slower volume coverage: Increased *N* and slower patient heart rate require a reduction in spiral pitch.

Multisegment approaches rely on a complete periodicity of the heart motion, and these approaches encounter their limitations in patients with arrhythmia or a heart rate that changes during scan acquisition. Multisegment reconstruction may improve image quality in selected cases, but the reliability of good-quality image acquisitions with *N*-segment reconstruction is compromised with increases in *N.*

In general, clinical practice suggests the use of one segment at lower heart rates and two or more ($N \geq 2$) segments at higher heart rates. Use of single-segment versus multisegment reconstruction is integrated in the data acquisition process in a variety of ways, depending on the scanner type. One approach consists of automatic division of the partial-scan data segment into one or two subsegments, depending on the patient's heart rate during acquisition ("adaptive cardio volume" algorithm [74]). With a different approach, single-segment partial-scan images are prospectively reconstructed as baseline images, followed by retrospective two-segment reconstruction for improved temporal resolution in patients with a higher heart rate. Yet another approach is prospective adjustment of the gantry rotation time to the heart rate of the patient to obtain an optimized temporal resolution for a multisegment reconstruction. Again, this approach requires a stable and predictable heart rate during scan acquisition.

Prospective ECG triggering combined with sequential step-and-shoot acquisition of transverse sections has the benefit of smaller patient dose than that of ECG-gated spiral scanning, because scan data are acquired only during the desired heart phases. However, this technique does not provide continuous volume coverage with overlapping sections, and misregistration of anatomic details cannot be avoided. Furthermore, reconstruction of images in different phases of the cardiac cycle for functional evaluation is not possible. Since ECG-triggered sequential scanning depends on a reliable prediction of the patient's next R-R interval by using the mean of the preceding R-R intervals, the method encounters its limitations in patients with arrhythmia. To maintain the benefits of ECG-gated spiral CT but reduce patient dose, ECG-controlled dose modulation has been developed (42,43) (see earlier discussion).

The major improvements of 16-section CT, compared with established four-section scanners, include improved temporal resolution due to shorter gantry rotation time, better spatial resolution owing to submillimeter collimation, and considerably reduced scan acquisition times (26,27). The time to cover the entire heart volume (about 12 cm) with four-section CT at 1.0-mm collimation is about 40 seconds, which is at the limit for a scan requiring patient breath holding. ECG-gated CT of the entire thorax or the aorta is not possible within reasonable scan durations. For a 16-section CT system, the time to cover the entire heart volume with submillimeter collimation is about 15 seconds. With 16-section CT, coverage of the entire thorax (30 cm) can be completed in about 38 seconds at 0.75-mm collimation and in about 19 seconds at 1.5-mm collimation. ECG-gated examinations of extended cardiothoracic anatomy became feasible with 16-section CT, which lends itself to a spectrum of applications where suppression of cardiac pulsation is desired. Typical diagnostic pitfalls caused by transmitted cardiac pulsation can be avoided, such as an artifactual intimal flap resembling dissection in the ascending aorta (79). Suppression of cardiac pulsation improves the assessment of paracardiac lung segments and allows confident exclusion of small peripheral pulmonary emboli in segmental and subsegmental arteries (80). In routine thoracic studies, which are not synchronized to the patient's ECG signal, cardiac motion usually precludes the assessment of coronary bypass grafts. Figure 16 shows an example of an ECG-gated scan of the entire thorax for a patient with bypass grafts; this scan was acquired with 16-section CT at 0.75-mm collimation and 0.42-second gantry rotation.

APPLICATIONS

Clinical applications benefit from multi–detector row CT technology in several ways: *(a)* shorter scan time (important for trauma patients and pediatric patients, CT angiography), *(b)* extended scan range (important for CT angiography, combined chest-abdomen scans such as in oncologic staging), and *(c)* improved longitudinal resolution (beneficial for all reconstructions,

particularly when 3D postprocessing is part of the clinical protocol).

Most protocols even benefit from a combination of all of these advantages. The near isotropic spatial resolution in routine examinations enables 3D renderings of diagnostic quality and oblique MPRs and maximum intensity projections of a resolution similar to that of the transverse images. The availability of multi–detector row CT technology has already begun to change the traditional perception of CT imaging. In CT, a distinction is traditionally made between longitudinal and in-plane resolution. This distinction is based mainly on historical reasons. Before the introduction of spiral CT, longitudinal resolution was determined by section collimation alone, while the convolution kernel determined in-plane resolution. With spiral CT, collimation is no longer the only factor used to determine longitudinal resolution; the spiral interpolation function also comes into play. This has been a first step toward decoupling the image section width from the beam width as determined by the collimation. Multi–detector row CT now allows reconstruction of arbitrary section widths from a given collimation by using z-filter techniques, as long as the desired section width is not smaller than the collimation. The potential to trade off z-axis resolution and image noise for the same data set is the most important benefit of z-filter reconstruction. In many applications, data acquisition with narrow collimation is recommended independently of the section width desired for primary viewing.

The distinction between longitudinal and in-plane resolution will gradually become a historical curiosity, and the traditional transverse section will loose its clinical importance. In its place, interactive viewing and manipulation of isotropic volume images will become commonplace, with only the key sections or views in arbitrary directions recorded and stored.

Spiral scanning with 16 submillimeter sections, in particular, represents a breakthrough on the way to true isotropic resolution for routine clinical applications. Improved longitudinal resolution is combined with considerably reduced scan times, which facilitate examinations in uncooperative patients and reduce the amount of contrast material needed (although optimized contrast material protocols are also required).

Furthermore, new clinical applications are evolving as a result of the increased speed of volume scanning. CT angiography of the carotid arteries and the circle of Willis with 16 sections at 0.75-mm collimation, 0.5-second rotation time, and pitch of 1.5 requires only 9 seconds for a scan range of about 300 mm (with table feed of 36 mm/sec). For the first time, true arterial phase imaging of the entire carotid artery with high spatial resolution can be performed. Clinical practice indicates the potential of 16-section CT angiography to replace conventional interventional angiography in the evaluation of carotid artery stenosis (81). Evaluation of the supraaortic vessels with 16-section CT is particularly useful in emergency situations, since CT allows a quick diagnosis with optimized patient access.

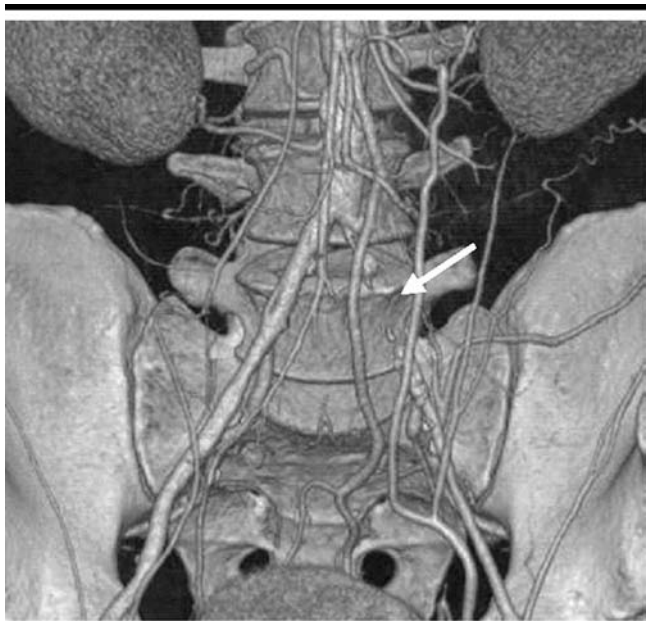

Figure 17. Clinical performance of 16-section CT (0.75-mm collimation, 0.5-second gantry rotation). Coronal volume-rendered reconstruction shows occlusion of left common iliac artery (arrow). (Image courtesy of Axel Küttner, MD, University of Tübingen, Germany.)

For patients suspected of having ischemic stroke, both the status of the vessels supplying the brain and the location of the intracranial occlusion can be assessed during the same examination (82). Brain perfusion CT can be performed by using the same modality, with the goal of differentiating irreversibly damaged brain tissue from reversibly impaired tissue at risk. The combined use of nonenhanced CT, perfusion CT, and CT angiography may rapidly provide comprehensive information regarding the extent of ischemic damage in patients with acute stroke (46).

Scan acquisition of the entire thorax (350 mm) with submillimeter collimation can now be performed in approximately 11 seconds. Owing to the short breathhold time, central and peripheral pulmonary embolism can be reliably and accurately diagnosed even in severely dyspneic patients with limited ability to cooperate (11,83). Meanwhile the use of multi–detector row CT for a combined diagnosis of pulmonary embolism and deep venous thrombosis has been clinically established (83). Both a native and a contrast-enhanced scan of the thorax can be obtained within the same breath hold for matching of both image volumes as a basis for investigational applications such as lung perfusion imaging.

Sixteen-section CT enables whole body angiographic studies with submillimeter resolution in a single breath hold. Also, 16-section CT yields the same morphologic information as invasive angiography (84,85). CT angiography of the chest and abdomen with submillimeter collimation can be completed in about 17 seconds for a scan range of 600 mm (Fig 17). When true isotropic resolution is not required, the use of 16-section CT at 1.25- or 1.5-mm collimation enables even shorter examination times or extended scan ranges (eg, for oncologic screening, trauma cases, or CT angiography). Whole-body 16-section CT angiography with 1500-mm scan range, 1.5-mm collimation, 0.5-second rotation time, and pitch of 1.25 (table feed, 60 mm/sec) can be completed in only 26 seconds.

ECG-gated cardiac scanning benefits from both improved temporal resolution and improved spatial resolution. Detection and characterization of coronary

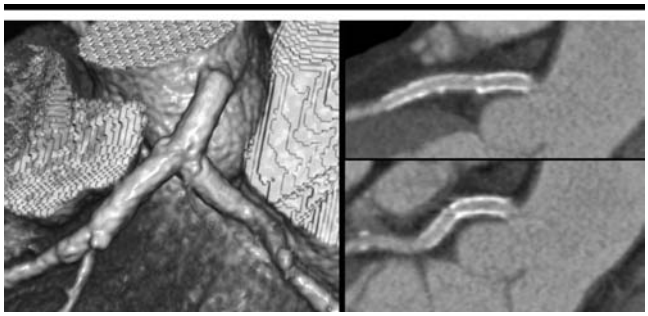

Figure 18. Clinical performance of ECG-gated 16-section coronary CT angiography (0.75-mm collimation, 0.37-second gantry rotation). Images of patient after insertion of Y stent into bifurcation of left main coronary artery into left anterior descending and left circumflex coronary arteries. Mean heart rate of the patient during examination was 67 beats per minute. Left: Y stent is shown in 3D volume-rendered reconstruction. Right: Multiplanar reformations of left anterior descending and circumflex arteries demonstrate stent patency with sufficient diagnostic quality to obviate invasive coronary angiography. (Image courtesy of Filippo Cademartiri, MD, Thorax Center Rotterdam, the Netherlands.)

plaque, even in the presence of severe calcifications, greatly benefits from the increased robustness of the technology. Sixteen-section CT allows assessment of small, peripheral coronary segments that, until now, could not be evaluated. In a recent study (86) in which coronary CT angiography with a 16-section system was investigated in 59 patients, 86% specificity and 95% sensitivity were demonstrated for identification of significant coronary artery stenosis. None of the patients had to be excluded, unlike in previous studies that were based on less-advanced scanner technology. Other investigators have reported similar results (87). Early clinical experience with 0.37-second gantry rotation indicates improved image quality due to reduced cardiac motion and increased clinical robustness at higher heart rates, which thereby potentially reduce the number of patients who require heart rate control (Fig 18).

FUTURE DIRECTION OF MULTI–DETECTOR ROW CT

Sixteen-section CT, which has become widely available, enables truly isotropic submillimeter imaging for virtually any application. In the case of cardiac imaging, 16-section CT sets today's benchmark in spatial resolution for noninvasive coronary artery imaging. Motion artifacts in patients with a higher heart rate remain the most important challenge for multi–detector row coronary CT angiography, although diagnostic image quality can be achieved in most cases by administering β-blockers to such patients. Improved temporal resolution is desirable in the future to prevent the need for heart rate control. Increased gantry rotation speed, rather than multisegment reconstruction, appears to be preferable for robust clinical performance. Obviously, substantial development efforts are needed to account for the notable increase in mechanical forces (about $17g$ for 0.42-second rotation, $>33g$ for 0.3-second rotation) and increased data transmission rates. A rotation time of less than 0.2 second (mechanical force $> 75g$), which is required to provide a temporal resolution of less than 100 msec independent of heart rate, appears to be beyond today's mechanical limits. An alternative to further increases in rotation speed is to reconsider the scanner concept with multiple tubes and multiple detectors that had already been described in the early years of CT (88,89).

Owing to its ease of use and its widespread availability, general-purpose CT continues to evolve into the most widely used diagnostic modality for routine examinations, especially in emergency situations or for oncologic staging. CT primarily provides morphologic information; in combination with other modalities, however, functional and metabolic information can also be obtained (90). Therefore, combined systems for obtaining comprehensive structural and functional diagnoses will gain increasing importance in the near future.

The combination of state-of-the-art multi–detector row CT with positron emission tomographic (PET) scanners, for instance, opens a wide spectrum of applications ranging from oncologic staging to comprehensive cardiac examinations. The clinical potential of these scanners is currently being evaluated (91). Reconstruction of the CT images in a sufficient field of view without truncation of anatomic structures (eg, arms) is a prerequisite for adequate attenuation correction of the PET images. An enlarged field of view of up to 70 cm can be realized by extrapolating from the measured CT data. Pertinent algorithms can be found in, for example, reference 92. Figure 19 shows MPRs from CT images in a 46-year-old man with renal cancer who had undergone nephrectomy and chemotherapy, with PET images superimposed. Areas with increased metabolism are enhanced, and a metastatic mediastinal lymph node can be identified, which supports the notion of PET as adding a "new contrast agent" to CT.

Systems that combine CT and single-photon emission computed tomography are another promising modality. Potential applications are currently being investigated and range from the localization of parathyroid lesions (93) and heterotopic splenic tissue (94) to detection of recurrent nasopharyngeal carcinomas (95) to imaging of aortic prosthesis infection (96).

CT virtual simulation is gaining increasing importance with a more widespread adoption in 3D conformal and intensity-modulated radiation therapy. With general-purpose CT systems that have a gantry opening with a typical diameter of 70 cm, some patients (eg, women with breast cancer) cannot always be scanned in the treatment position. Such applications, along with interventional procedures and trauma protocols, will be facilitated by CT systems with a larger bore (97). Recently, concepts have been introduced for four- and 16-section CT scanners with a bore diameter of up to 85 cm and a reconstruction field of up to 82 cm, owing to image reconstruction based on data extrapolation. These systems will probably gain considerable importance in the near future, in particular with regard to the dramatically increasing number of severely obese patients in the Western countries.

For general purpose CT, we will witness a moderate increase in the number of simultaneously acquired sections in the near future. A new generation of CT systems with 32, 40 and—in combination with refined *z*-axis sampling techniques—64 simultaneously acquired sections are currently being introduced. However in contrast to

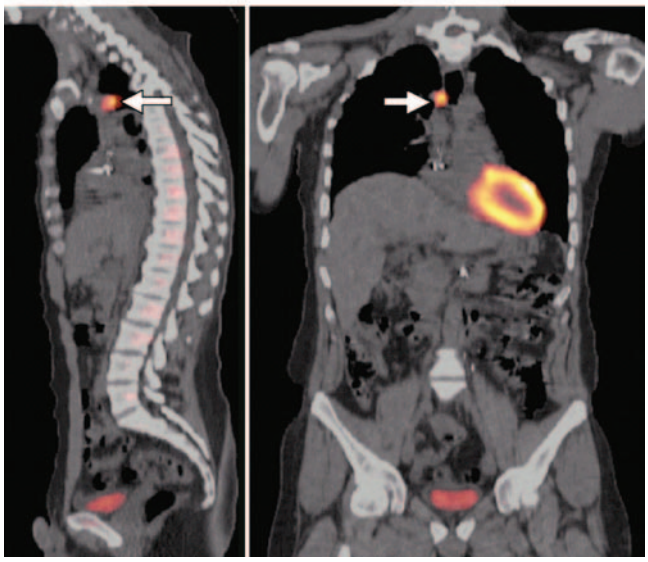

Figure 19. Clinical performance of PET/CT. Sagittal (left) and coronal (right) MPRs from CT data in patient with renal cancer, with PET images superimposed. Areas with enhanced metabolism show more avid tracer accumulation. Metastatic mediastinal lymph node (arrows) can be identified.

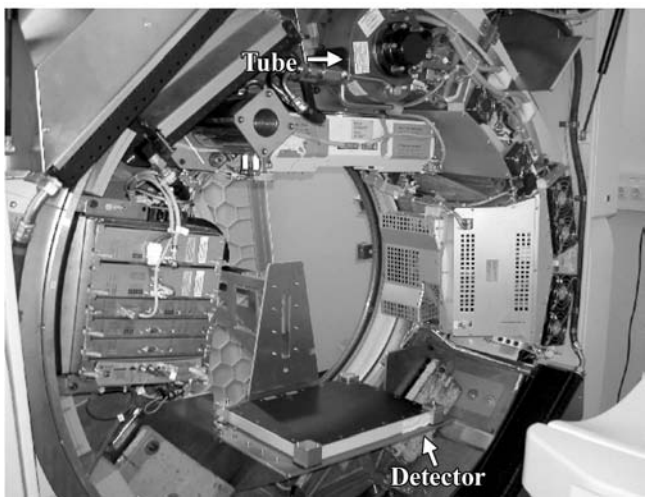

Figure 20. Prototype CT system incorporates cesium iodide flat-panel detector into a standard CT gantry.

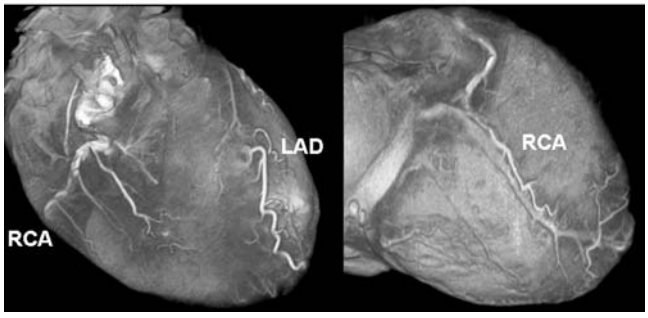

Figure 21. Volume-rendered display of stationary heart specimen scanned with flat-panel CT prototype with cesium iodide detector shown in Figure 20. The 0.25-mm^3 isotropic resolution enables exquisite delineation of small side branches of contrast material–filled coronary artery tree. *LAD* = left anterior descending coronary artery, *RCA* = right main coronary artery.

the transition from single-section to four- and 16-section CT, clinical performance will improve only incrementally with further increases in the number of detector rows. The achievable clinical benefit will have to be carefully considered in the light of the necessary technical efforts and the cost. Clinical progress can more likely be expected from further improvements in spatial resolution rather than from an increase in the volume-coverage speed. In clinical reality, the latter has only rarely been a limiting factor since the introduction of 16-section CT. As soon as all relevant examinations can be performed in a comfortable breath hold of not more than 10 seconds, a further increase in the number of sections will not provide a substantial clinical benefit.

At this point, a qualitative enhancement of CT that allows new clinical applications may again bring substantial clinical progress with, for example, the introduction of area detectors large enough to cover entire organs such as the heart, kidneys, or brain in one sequential scan (approximate scan range, 120 mm). With these systems, dynamic volume scanning would become feasible, which would open up a whole spectrum of new applications such as functional or volume perfusion studies.

Area-detector technology is currently under development, but no commercially available system so far fulfills the requirements of medical CT with regard to contrast resolution and fast data readout. A scanner with 256 0.5-mm detector elements has been proposed by one manufacturer and appears to be conceptually promising, but this system is still in the prototype stage. Prototype systems by other vendors use cesium iodide–amorphous silicon flat-panel detector technology that was originally used for conventional angiography, which is limited in terms of low contrast resolution and imaging speed. Owing to the intrinsic slow signal decay of flat-panel detectors, rotation times of at least 20 seconds are needed to acquire a sufficient number of projections (≥600 projections). The spatial resolution of such systems is excellent, though, because of the small detector pixel size. Excessive dose requirements to date, however, preclude the examination of larger objects. Initial experimental results are thus limited to small high-contrast objects such as joints, the inner ear, or contrast material–filled vessel specimens (98,99).

Figure 20 shows a prototype set-up, where a flat-panel detector was incorporated into a standard CT gantry (Somatom Sensation 16; Siemens). The detector covers a 25 × 25 × 18 cm scan field of view, and the pixel size is 0.25 × 0.25 mm, both measured at the center of rotation. Figure 21 shows volume renderings of a heart specimen (80 kV, 20 mA, 20-second gantry rotation) that demonstrate excellent spatial resolution, which enables visualization of even very small side branches of the coronary artery tree.

The combination of area detectors that provide sufficient image quality with fast gantry rotation speed will be a promising technical concept for medical CT systems. The vast spectrum of potential applications may bring about another

quantum leap in the evolution of medical CT imaging; however such systems will probably not be available in the near future.

References

1. Kalender W, Seissler W, Klotz E, Vock P. Spiral volumetric CT with single-breath-hold technique, continuous transport, and continuous scanner rotation. Radiology 1990; 176:181–183.
2. Crawford CR, King KF. Computed tomography scanning with simultaneous patient translation. Med Phys 1990; 17:967–982.
3. Rubin GD, Dake MD, Semba CP. Current status of three-dimensional spiral CT scanning for imaging the vasculature. Radiol Clin North Am 1995; 33:51–70.
4. Napel S, Rubin GD, Jeffrey RB. STS-MIP: a new reconstruction technique for CT of the chest. J Comput Assist Tomogr 1993; 17:832–838.
5. Kalender W. Thin-section three-dimensional spiral CT: is isotropic imaging possible? (editorial). Radiology 1995; 197:578–580.
6. Liang Y, Kruger RA. Dual-slice spiral versus single-slice spiral scanning: comparison of the physical performance of two computed tomography scanners. Med Phys 1996; 23: 205–220.
7. Klingenbeck-Regn K, Schaller S, Flohr T, Ohnesorge B, Kopp AF, Baum U. Subsecond multi-slice computed tomography: basics and applications. Eur J Radiol 1999; 31:110–124.
8. Hu H, He HD, Foley WD, Fox SH. Four multidetector-row helical CT: image quality and volume coverage speed. Radiology 2000; 215:55–62.
9. Ohnesorge B, Flohr T, Schaller S, et al. Technische grundlagen und anwendungen der mehrschicht-CT. Radiologe 1999; 39:923–931.
10. McCollough CH, Zink FE. Performance evaluation of a multidetector row CT system. Med Phys 1999; 26:2223–2230.
11. Remy-Jardin M, Tillie-Leblond I, Szapiro D, et al. CT angiography of pulmonary embolism in patients with underlying respiratory disease: impact of multislice CT on image quality and negative predictive values. Eur Radiol 2002; 12:1971–1978.
12. Rubin GD, Schmidt AJ, Logan LJ, Sofilos MC. Multi–detector row CT angiography of lower extremity arterial inflow and runoff: initial experience. Radiology 2001; 221:146–158.
13. Schoepf UJ, Bruening RD, Hong C, et al. Multislice helical CT of focal and diffuse lung disease: comprehensive diagnosis with reconstruction of contiguous and high-resolution CT sections from a single thin-collimation scan. AJR Am J Roentgenol 2001; 177: 179–184.
14. Villablanca JP, Lahan R, Hooshi P, et al. Detection and characterization of very small cerebral aneurysms by using 2D and 3D helical CT angiography. AJNR Am J Neuroradiol 2002; 23:1187–1198.
15. Flohr T, Stierstorfer K, Bruder H, Simon J, Schaller S. New technical developments in multislice CT. I. Approaching isotropic resolution with sub-mm 16-slice scanning. Rofo Fortschr Geb Rontgenstr Neuen Bildgeb Verfahr 2002; 174:839–845.
16. Kachelriess M, Ulzheimer S, Kalender W. ECG-correlated image reconstruction from subsecond multi-slice spiral CT scans of the heart. Med Phys 2000; 27:1881–1902.
17. Ohnesorge B, Flohr T, Becker C, et al. Cardiac imaging by means of electrocardiographically gated multisection spiral CT: initial experience. Radiology 2000; 217:564–571.
18. Hong C, Becker CR, Huber A, et al. ECG-gated reconstructed multi–detector row CT coronary angiography: effect of varying trigger delay on image quality. Radiology 2001; 220:712–717.
19. Achenbach S, Ulzheimer S, Baum U, et al. Noninvasive coronary angiography by retrospectively ECG-gated multi-slice spiral CT. Circulation 2000; 102:2823–2828.
20. Becker C, Knez A, Ohnesorge B, Schöpf U, Reiser M. Imaging of non calcified coronary plaques using helical CT with retrospective EKG gating. AJR Am J Roentgenol 2000; 175: 423–424.
21. Knez A, Becker C, Leber A, Ohnesorge B, Reiser M, Haberl R. Non-invasive assessment of coronary artery stenoses with multidetector helical computed tomography. Circulation 2000; 101:e221–e222.
22. Nieman K, Oudkerk M, Rensing BJ, et al. Coronary angiography with multi-slice computed tomography. Lancet 2001; 357:599–603.
23. Schroeder S, Kopp A, Baumbach A, et al. Noninvasive detection and evaluation of atherosclerotic coronary plaques with multislice computed tomography. J Am Coll Cardiol 2001; 37:1430–1435.
24. Schroeder S, Flohr T, Kopp AF, et al. Accuracy of density measurements within plaques located in artificial coronary arteries by x-ray multislice CT: results of a phantom study. J Comput Assist Tomogr 2001; 25:900–906.
25. Kopp A, Schröder S, Küttner A, et al. Coronary arteries: retrospectively ECG-gated multi–detector row CT angiography with selective optimization of the image reconstruction window. Radiology 2001; 221: 683–688.
26. Flohr T, Bruder H, Stierstorfer K, Simon J, Schaller S, Ohnesorge B. New technical developments in multislice CT. II. Sub-millimeter 16-slice scanning and increased gantry rotation speed for cardiac imaging. Rofo Fortschr Geb Rontgenstr Neuen Bildgeb Verfahr 2002; 174:1022–1027.
27. Flohr T, Schoepf UJ, Kuettner A, et al. Advances in cardiac imaging with 16-section CT-systems. Acad Radiol 2003; 10:386–401.
28. Schoepf UJ, Becker CR, Ohnesorge BM, Yucel EK. CT of coronary artery disease. Radiology 2004; 232:18–37.
29. Hu H. Multi-slice helical CT: Scan and reconstruction. Med Phys 1999; 26:5–18.
30. Brenner D, Elliston C, Hall E, Berdon W. Estimated risks of radiation-induced fatal cancer from pediatric CT. AJR Am J Roentgenol 2001; 176:289–296.
31. Nickoloff E, Alderson P. Radiation exposure to patients from CT: reality, public perception, and policy. AJR Am J Roentgenol 2001; 177:285–287.
32. McCollough C. Patient dose in cardiac computed tomography. Herz 2003; 28:1–6.
33. Morin R, Gerber T, McCollough C. Radiation dose in computed tomography of the heart. Circulation 2003; 107:917–922.
34. International Electrotechnical Commission 60601–2–44. Amendment 1: medical electrical equipment, part 2–44: particular requirements for the safety of x-ray equipment for computed tomography. Geneva, Switzerland: International Electrotechnical Commission, 2002.
35. Donnelly LF, Emery KH, Brody AS, et al. Minimizing radiation dose for pediatric body applications of single-detector helical CT: strategies at a large children's hospital. AJR Am J Roentgenol 2001; 176:303–306.
36. Frush DP, Soden B, Frush KS, Lowry C. Improved pediatric multidetector body CT using a size-based color-coded format. AJR Am J Roentgenol 2002; 178:721–726.
37. Wildberger JE, Mahnken AH, Schmitz-Rode T, et al. Individually adapted examination protocols for reduction of radiation exposure in chest CT. Invest Radiol 2001; 36:604–611.
38. Schaller S, Niethammer MU, Chen X, Klotz E, Wildberger JE, Flohr T. Comparison of signal-to-noise and dose values at different tube voltages for protocol optimization in pediatric CT (abstr). Radiology 2001; 221(P):366.
39. Wintersperger B, Becker CR, Schaller S, Rist C, Jakobs TF, Reiser MF. Low dose 16-detector-row CT angiography of the abdominal vessels with improved vessel enhancement (abstr). In: Radiological Society of North America scientific assembly and annual meeting program. Oak Brook, Ill: Radiological Society of North America, 2003; 541–542.
40. Kalender WA, Wolf H, Suess C. Dose reduction in CT by anatomically adapted tube current modulation. II. Phantom measurements. Med Phys 1999; 26:2248–2253.
41. Greess H, Wolf H, Baum U, et al. Dose reduction in computed tomography by attenuation-based on-line modulation of the tube current: evaluation of six anatomical regions. Eur Radiol 2000; 10:391–394.
42. Jakobs TF, Becker CR, Ohnesorge B, et al. Multislice helical CT of the heart with retrospective ECG gating: reduction of radiation exposure by ECG-controlled tube current modulation. Eur Radiol 2002; 12:1081–1086.
43. Poll L, Cohnen M, Brachten S, Ewen K, Modder U. Dose reduction in multidetector row CT of the heart by use of ECG-controlled tube current modulation ("ECG pulsing"): phantom measurements. Rofo Fortschr Geb Rontgenstr Neuen Bildgeb Verfahr 2002; 174:1500–1505.
44. Hsieh J. Investigation of the slice sensitivity profile for step-and-shoot mode multi-slice computed tomography. Med Phys 2001; 28: 491–500.
45. Joseph PM, Spital RD. The exponential edge-gradient effect in x-ray computed tomography. Phys Med Biol 1981; 26:473–487.
46. Tomandl BF, Klotz E, Handschu R, et al. Comprehensive imaging of ischemic stroke with multisection CT. RadioGraphics 2003; 23:565–592.
47. Polacin A, Kalender WA, Marchal G. Evaluation of section sensitivity profiles and image noise in spiral CT. Radiology 1992; 185:29–35.
48. Rubin GD, Napel S. Increased scan pitch for vascular and thoracic spiral CT. Radiology 1995; 197:316–317.
49. Saito Y, Suzuki T. Evaluation of the performance of multidetector row CT system in non-helical scanning (abstr). Radiology 1998; 209(P):578.
50. Hsieh J. Analytical models for multi-slice helical CT performance parameters. Med Phys 2003; 30:169–178.
51. Schaller S, Flohr T, Klingenbeck K, Krause J, Fuchs T, Kalender WA. Spiral interpolation algorithm for multi-slice spiral CT. I. Theory. IEEE Trans Med Imaging 2000; 19:822–834.
52. Taguchi K, Aradate H. Algorithm for image reconstruction in multi-slice helical CT. Med Phys 1998; 25:550–561.
53. Flohr T, Klingenbeck-Regn K, Ohnesorge B, Schaller S. Multislice scanning with the Somatom Volume Zoom: an optimized design for volume scanning. In: Reiser MF, Takahashi M, Modic M, Bruening R, eds. Multislice CT: medical radiology—diagnostic imaging and radiation oncology. Berlin, Germany: Springer-Verlag, 2001.
54. Fuchs T, Krause J, Schaller S, Flohr T, Kalender WA. Spiral interpolation algorithms for multislice spiral CT. II. Measurement and evaluation of slice sensitivity pro-

files and noise at a clinical multislice system. IEEE Trans Med Imaging 2000; 19:835–847.
55. Schaller S, Ohnesorge B, Flohr T, Klingenbeck-Regn K. Dose in multislice spiral CT (abstr). Radiology 1999; 213(P):284.
56. Wessling J, Fischbach R, Ludwig K, et al. Multi-slice spiral CT of the abdomen in oncological patients: influence of table support and detector configuration on image quality and radiation exposure. Rofo Fortschr Geb Rontgenstr Neuen Bildgeb Verfahr 2001; 173:373–378.
57. Feldkamp LA, Davis LC, Kress JW. Practical cone-beam algorithm. J Opt Soc Am A 1984; 1:612–619.
58. Grass M, Köhler T, Proksa R. 3D cone-beam CT reconstruction for circular trajectories. Phys Med Biol 2000; 45:329–347.
59. Wang G, Lin T, Cheng P. A general cone-beam reconstruction algorithm. IEEE Trans Med Imaging 1993; 12:486–496.
60. Schaller S. Practical image reconstruction for cone-beam computed tomography (dissertation). Nürnberg, Germany: Erlangen University; 1998.
61. Turbell H, Danielsson PE. An improved PI-method for reconstruction from helical cone beam projections. Presented at the IEEE Medical Imaging Conference, Seattle, Wash, October 24–30, 1999.
62. Proksa R, Koehler T, Grass M, Timmer J. The n-PI method for helical cone-beam CT. IEEE Trans Med Imaging 2000; 19:848–863.
63. Larson G, Ruth C, Crawford C. Nutating slice CT image reconstruction. U.S. patent application WO 98/44847; filed April 8, 1998.
64. Kachelriess M, Schaller S, Kalender WA. Advanced single-slice rebinning in cone-beam spiral CT. Med Phys 2000; 27:754–772.
65. Bruder H, Kachelriess M, Schaller S, Stierstorfer K, Flohr T. Single-slice rebinning reconstruction in spiral cone-beam computed tomography. IEEE Trans Med Imaging 2000; 19:873–887.
66. Kohler T, Proksa R, Bontus C, Grass M, Timmer J. Artifact analysis of approximate helical cone-beam CT reconstruction algorithms. Med Phys 2002; 29:51–64.
67. Schaller S, Stierstorfer K, Bruder H, Kachelriess M, Flohr T. Novel approximate approach for high-quality image reconstruction in helical cone beam CT at arbitrary pitch. In: Sonka M, Hanson KM, eds. Proceedings of SPIE: medical imaging 2001—image processing. Vol 4322. Bellingham, Wash: International Society for Optical Engineering, 2001; 113–127.
68. Flohr T, Stierstorfer K, Bruder H, Simon J, Polacin A, Schaller S. Image reconstruction and image quality evaluation for a 16-slice CT scanner. Med Phys 2003; 30:832–845.
69. Hsieh J, Toth TL, Simoni P, Grekowicz B, Slack CC, Seidenschnur GE. A generalized helical reconstruction algorithm for multidetector row CT (abstr). Radiology 2001; 221(P):217.
70. Hsieh J, Grekowicz B, Simoni P, et al. Convolution reconstruction algorithm for multislice helical CT. In: Sonka M, Fitzpatrick MJ, eds. Proceedings of SPIE: medical imaging 2003—image processing. Vol 5032. Bellingham, Wash: International Society for Optical Engineering, 2003; 716–723.
71. Stierstorfer K, Flohr T, Bruder H. Segmented multiple plane reconstruction: a novel approximate reconstruction scheme for multislice spiral CT. Phys Med Biol 2002; 47:2571–2581.
72. Toth TL, Simoni P. A quantitative measure of CT helical artifact (abstr). Radiology 2001; 221(P):218.
73. Kachelriess M, Kalender W. Electrocardiogram-correlated image reconstruction from subsecond spiral computed tomography scans of the heart. Med Phys 1998; 25:2417–2431.
74. Flohr T, Ohnesorge B. Heart-rate adaptive optimization of spatial and temporal resolution for ECG-gated multi-slice spiral CT of the heart. J Comput Assist Tomogr 2001; 25: 907–923.
75. Taguchi K, Anno H. High temporal resolution for multi-slice helical computed tomography. Med Phys 2000; 27:861–872.
76. Bruder H, Schaller S, Ohnesorge B, Mertelmeier T. High temporal resolution volume heart imaging with multirow computed tomography. In: Hanson KM, ed. Proceedings of SPIE: medical imaging 1999—image processing. Vol 3661. Bellingham, Wash: International Society for Optical Engineering, 1999; 420–432.
77. Pan T, Shen Y. New multi-sector reconstruction for cardiac ct. Presented at IEEE Medical Imaging Conference, Lyon, France, October 16–20, 2000.
78. Cesmeli E, Edic M, Iatrou M, Pfoh A. A novel reconstruction algorithm for multiphasic cardiac imaging using multislice CT. In: Antonuk LE, Yaffe MJ, eds. Proceedings of SPIE: medical imaging 2001—physics of medical imaging. Vol 4320. Bellingham, Wash: International Society for Optical Engineering; 645–654.
79. Loubeyre P, Angelie E, Grozel F, Abidi H, Minh VA. Spiral CT Artifact that simulates aortic dissection: image reconstruction with use of 180° and 360° linear-interpolation algorithms. Radiology 1997; 205:153–157.
80. Schoepf U, Helmberger T, Holzknecht N, et al. Segmental and subsegmental pulmonary arteries: evaluation with electron-beam CT versus spiral CT. Radiology 2000; 214:433–439.
81. Lell M, Wildberger J, Heuschmid M, et al. CT-angiography of the carotid artery: first results with a novel 16-slice-spiral-CT scanner. Rofo Fortschr Geb Rontgenstr Neuen Bildgeb Verfahr 2002; 174:1165–1169.
82. Ertl-Wagner B, Hoffmann RT, Brüning R, Dichgans M, Reiser MF. Supraaortale gefässdiagnostik mit dem 16-zeilen-multidetektor-spiral-CT: untersuchungsprotokoll und erste erfahrungen. Radiologe 2002; 42:728–732.
83. Schoepf UJ, Becker CR, Hofmann LK, et al. Multislice CT angiography. Eur Radiol 2003; 13:1946–1961.
84. Wintersperger B, Helmberger T, Herzog P, et al. New abdominal CT angiography protocol on a 16 detector-row CT scanner. Radiologe 2002; 42:722–727.
85. Wintersperger B, Herzog P, Jakobs T, Reiser M, Becker C. Initial experience with the clinical use of a 16 detector row CT system. Crit Rev Comput Tomogr 2002; 43:283–316.
86. Nieman K, Cademartiri F, Lemos PA, Raaijmakers R, Pattynama PM, de Feyter PJ. Reliable noninvasive coronary angiography with fast submillimeter multislice spiral computed tomography. Circulation 2002; 106: 2051–2054.
87. Ropers D, Baum U, Pohle K, et al. Detection of coronary artery stenoses with thin-slice multi-detector row spiral computed tomography and multiplanar reconstruction. Circulation 2003; 107:664–666.
88. Robb R, Ritman E. High speed synchronous volume computed tomography of the heart. Radiology 1979; 133:655–661.
89. Ritman E, Kinsey J, Robb R, Gilbert B, Harris L, Wood E. Three-dimensional imaging of heart, lungs, and circulation. Science 1980; 210:273–280.
90. Townsend DW, Cherry SR. Combining anatomy and function: the path of true image fusion. Eur Radiol 2001; 11:1968–1974.
91. Namdar M, Kaufmann P, Hany T, von Schulthess G. Combined CT-angiogram and PET perfusion imaging for assessment of CAD in a novel PET/CT: a pilot feasibility study (abstr). Eur Radiol 2003; 13(suppl):165.
92. Ohnesorge B, Flohr T, Schwarz K, Heiken JP, Bae KT. Efficient correction for CT image artifacts caused by objects extending outside the scan field of view. Med Phys 2000; 27: 39–46.
93. Kaczirek K, Prager G, Kienast O, et al. Combined transmission and (99m)Tc-sestamibi emission tomography for localization of mediastinal parathyroid glands. Nuklearmedizin 2003; 42:220–223.
94. Horger M, Eschmann SM, Lengerke C, Claussen CD, Pfannenberg C, Bares R. Improved detection of splenosis in patients with haematological disorders: the role of combined transmission-emission tomography. Eur J Nucl Med Mol Imaging 2003; 30:316–319.
95. Tai CJ, Shian YC, Wang IJ, Ho YJ, Ho ST, Kao CH. Detection of recurrent or residual nasopharyngeal carcinomas after radiotherapy with technetium-99m tetrofosmin single photon emission computed tomography and comparison with computed tomography: a preliminary study. Cancer Invest 2003; 21: 536–541.
96. Hofmann A, Zettinig G, Wachter S, Kurtaran A, Kainberger F, Dudczak R. Imaging of aortic prosthesis infection with a combined SPECT/CT device. Eur J Nucl Med Mol Imaging 2002; 29:836.
97. Garcia-Ramirez JL, Mutic S, Dempsey JF, Low DA, Purdy JA. Performance evaluation of an 85-cm-bore x-ray computed tomography scanner designed for radiation oncology and comparison with current diagnostic CT scanners. Int J Radiat Oncol Biol Phys 2002; 52: 1123–1131.
98. Nikolaou K, Flohr T, Stierstorfer K, Becker CR, Reiser MF. Flat panel computed tomography of human ex vivo heart and bone specimens: initial experience. Eur Radiol 2005; 15:329–333.
99. Knollmann F, Pfoh A. Image in cardiovascular medicine: coronary artery imaging with flat-panel computed tomography. Circulation 2003; 107:1209.